Starch Nanoparticles for Targeted Anti-Cancer Drug Delivery

by

Tsung Hao Tsai

A thesis

presented to the University of Waterloo

in fulfillment of the

thesis requirement for the degree of

Master of Science

in

Chemistry

Waterloo, Ontario, Canada, 2015

Author's Declaration

I hereby declare that I am the sole author of this thesis. This is the true copy of the thesis, including any required final revisions, as accepted by my examiners. I understand that my thesis may be made electronically available to the public.

Abstract

In the field of anti-cancer drug delivery, nanoparticles have become an active topic of research. Nanoparticles made of biodegradable materials such as polylactic acid, proteins, and polysaccharides have been reported for delivery applications. Among all the studies, polysaccharide-based systems are gaining increasing attention due to their low toxicity, great abundance, and high biocompatibility. However, relatively few starch-based nanoparticle delivery systems have been reported. In addition, most previous work employed only small-scale lab synthesized starch nanoparticles, which were made under various condition using different crosslinking agents. Therefore, they may have large batch-to-batch variation. This thesis reports a starch nanoparticle delivery system designed to target cancer cells. A commercially available starch nanoparticle material named EcoSphere™ was modified with aptamers to achieve active targeting. Our EcoSphere™ nanoparticles (ENP) were made in very large scale and its modification scheme is divided into initial oxidation and subsequent aptamer conjugation. ENPs were first subject to TEMPO-mediated oxidation to selectively oxidize its C6 hydroxyl group into carboxyl group. Partially oxidized ENPs were confirmed and characterized through spectroscopic measurements, including NMR and dynamic light scattering. ENPs of various oxidation levels (1%, 2%, 5%, 10%, and 20%) were then tested for conjugation efficiency using dye molecules and control DNA, and only the 20% oxidized ENPs show minor DNA conjugation. DNA coupling procedure was then optimized and aptamer conjugation efficiency was improved to >80% by reacting at elevated temperatures and in slightly acidic environment. The fully modified ENPs were then subject to two cellular assays to evaluate cellular internalization and vehicle selectivity. Aptamer-modified ENPs show clear internalization and dye-modified ENPs also shows significant internalization. Vehicle selectivity was demonstrated through preferential uptake of AS1411-modified ENPs over sgc8-modified ENPs, where sgc8 is a control aptamer that does not target the HeLa cells.

Acknowledgments

I would like to express my sincere gratitude and appreciation to my supervisor, Dr. Juewen Liu. He is a knowledgeable and caring mentor who provided me with constant guidance and encouragement.

I would also like to thank the members of my committee Dr. Vivek Maheshwari and Dr. Shirley Tang for their time in reviewing my thesis and participating in my defense.

It was a pleasure working with my colleagues in Dr. Liu's lab. Everyone has helped me with technical problems or gave me advices at some point during the past two years. Special thanks to Dr. Feng Wang for technical guidance with cell culture and confocal microscopy, Jimmy Huang for denaturing PAGE training, Biwu Liu for assistance with fluorometer and UV-Vis spectrometer and Wenhu Zhou for DNA desalting.

I also want to acknowledge EcoSynthetix Inc for their technical and financial support. Special thanks to ECO-WIN professors and all the ECO-WIN members for their time and suggestion during quarterly meetings.

Lastly, I want to thank my family, friends, and girlfriend for their unconditional support.

Table of Contents

Author's Declaration ii
Abstract iii
Acknowledgements iv
Table of Contents v
List of Figures vii
List of Abbreviations x
Chapter 1. Introduction 1
1.1 Cancer 1
1.2 Cancer Therapy 2
1.2.1 Chemotherapy 3
1.3 Targeted Drug Delivery 6
1.3.1 Targeting Method 8
1.4 Nanoparticle Delivery System 10
1.5 Structure and Chemistry of Starch 12
1.6 Polysaccharides Delivery System 15
1.6.1 General Methods for Starch Nanoparticle Preparation 16
1.6.2 EcoSphere™ 17
1.7 Thesis Objective 18
Chapter 2. Oxidation of Starch Nanoparticles 21
2.1 TEMPO-mediated Oxidation of ENPs 21
2.2 Spectroscopic Characterization 23
2.2.1 NMR 23
2.2.2 DLS and Zeta-Potential 26
2.3 Materials and Methods 28
2.3.1 Materials 28
2.3.2 TEMPO-mediated Oxidation of ENPs 29
2.3.3 Spectroscopic Characterization 29

Chapter 3. DNA Conjugation 31
3.1 EDC/NHS-Mediated Aptamer Conjugation 31
3.1.1 Gel Electrophoresis Based Characterization 33
3.1.2 Optimization of Conjugation Efficiency 36
3.2 ENPs Precipitation 38
3.3 Materials and Methods 42
3.3.1 Materials 42
3.3.2 EDC/NHS Aptamer Conjugation 42
3.3.3 Gel Electrophoresis 43
Chapter 4. Cellular Uptake of ENPs 44
4.1 Cellular Internalization 44
4.2 Microscopic Imaging 45
4.2.1 Epifluorescence Microscopy 45
4.2.2 Confocal Laser Scanning Microscopy 47
4.3 Vehicle Internalization Assay 48
4.3.1 Aptamer Density 48
4.3.2 Duo Labeled Vehicle Assay 50
4.4 Vehicle Selectivity Assay 51
4.5 Internalization Efficacy Comparison - Liposome 53
4.6 Materials and Methods 55
4.6.1 Materials 55
4.6.2 Cell Culture 56
4.6.3 Confocal Laser Scanning Microscopy 56
4.6.4 Liposome Preparation 57
Chapter 5. Conclusion and Recommendations 58
5.1 Conclusion 58
5.2 Recommendations 60
References 63

List of Figures

Figure 1. Cancer death rate in the US, 1930-2008. This figure is adapted from ref. [7]. Copyright 2012, American Cancer Society 2

Figure 2. DNA alkylating agent mechanism of action. This figure is adapted from ref. [23]. Copyright 2013, Elsevier B.V. 5

Figure 3. Antimetabolites mimicking DNA building block nucleotide. This figure is adapted from ref. [28]. Copyright 2000, Elsevier B.V. 6

Figure 4. Enhanced permeability and retention effect. This figure is adapted from ref. [39]. Copyright 2010, SAGE Publications. 8

Figure 5. The SELEX system cycle. This figure is adapted from ref. [51]. Copyright 2015, Elsevier B.V. 10

Figure 6. Structures of amylose and amylopectin. This figure is adapted from ref. [65]. Copyright 2002, Elsevier B.V. 12

Figure 7. A- and B-type starch crystalline This figure is adapted from ref. [66]. Copyright 2004, Elsevier B.V. 13

Figure 8. Starch multi-scale structure. This figure is adapted from ref. [68]. Copyright 2010, American Chemical Society Publications. 14

Figure 9. Glyoxal crosslinking mechanism, R-OH represents the hydroxyl group on glucose[87]. 17

Figure 10. EcoSphereTM nanoparticle swollen structure. This figure is adapted from ref. [88]. Copyright 2004, Elsevier B.V. 18

Figure 11. Schematic for ENPs modification[89]. 19

Figure 12. TEMPO-mediated oxidation mechanism. This figure is adapted from ref. [90]. Copyright 2003, Elsevier B.V. 22

Figure 13. Oxidation level V.S. starch solubility in water. 23

Figure 14 . ^{1}H NMR spectrums of oxidized ENP samples. 25

Figure 15. ^{13}C NMR spectrum of 20% oxidized ENPs. 26

Figure 16. Size measurements of oxidized ENP samples at different pHs. The ENP concentration was 1% (w/w) 27

Figure 17. ζ-potential measurements of oxidized ENP samples at different pHs. The ENP concentration was 1% (w/w) 28

Figure 18. EDC/NHS conjugation mechanism. This figure is adapted from ref. [97]. Copyright 2008, Elsevier B.V. **32**

Figure 19. Denaturing PAGE results for dye coupled ENPs. First lane, HiLyte Fluor dye used as negative control. The next two lanes, 2% and 20% oxidized dextrin used as positive control. The remaining lanes show ENP samples of various oxidation levels. **34**

Figure 20. Denaturing PAGE results for control DNA coupled ENPs. First lane, Cy3-T15-NH_2 used as negative control. The next two lanes, 2% and 20% oxidized dextrin used as positive control. The remaining lanes show ENP samples of various oxidation levels..... **36**

Figure 21. Conjugation optimization result a) reaction time and pH b) temperature and DNA:ENP ratio. **37**

Figure 22. Aptamers and ENPs conjugation result a) denaturing PAGE results of aptamer coupled ENPs at two different concentration b) coupling efficiency quantification. **38**

Figure 23. ENPs precipitation test 1) 5% (w/w) dye-modified ENPs precipitated using ethanol. 2) 5% (w/w) dye-modified ENPs + non-labeled DNA precipitated with ethanol. 3) 5% (w/w) dye-modified ENPs + fluorophore-labeled DNA precipitated with ethanol. **40**

Figure 24. ENPs precipitation recovery assay. 5% (w/w) dye-modified ENPs precipitated with different solvents. Dye-modified ENPs mixed with different additive, then precipitated with ethanol. **41**

Figure 25. 5% (w/w) dye-modified ENP precipitated with 1) 100% isopropanol, 2) 100% ethanol, 3) 100% ethanol + 10 μL of 50 mM $MgCl_2$ salt. **42**

Figure 26. Proposed AS1411 mechanism of action[105]. AS1411 oligonucleotides dimerize to form eight G-quartets and interact with membrane nucleolin to trigger internalization. This figure is adapted from ref. [105]. Copyright 2006, American Association for Cancer Research. **45**

Figure 27. Epifluorescence microscopy images of cellular internalization assay. From top to bottom, aptamer-modified ENPs, random DNA-modified ENPs as negative control, and dye-modified 50 nm silicon beads as positive control..... **47**

Figure 28. Confocal microscopy images of cellular internalization assay. From top to bottom, aptamer-modified ENPs, random DNA-modified ENPs as negative control, and dye-modified 50 nm silicon beads as positive control. Blue channel shows stained nuclei, green channel shows fluorescent from aptamers, ENPs or silicon beads..... **48**

Figure 29. Internalization assay, aptamer density study. From top to bottom, dye-modified ENPs, high aptamer-ratio aptamer-modified ENPs, low aptamer-ratio aptamer-modified ENPs..... **49**

Figure 30. Internalization assay, duo labeled ENPs. From top to bottom, the negative control contained no samples, dye-modified ENPs, low aptamer-ratio aptamer-modified ENPs, high aptamer-ratio aptamer-modified ENPs. **51**

Figure 31. Vehicle selectivity assay. The first two samples are AS1411-modified ENPs (HeLa targeting) at two different aptamers:ENPs ratios. The bottom two samples are sgc8-modified ENPs (non-HeLa targeting) at the same two ratios. **53**

Figure 32. Internalization comparison, aptamer modified ENPs, aptamer modified liposomes and dye-labeled liposomes. **55**

List of Abbreviations

ADCs – antibody-drug conjugates

APS – ammonium persulfate

BSA – bovine serum albumin

DAPI – 4',6-diamidino-2-phenylindole

DLS – dynamic light scattering

DMEM – Dulbecco's Modified Eagle Medium

DNA – deoxyribonucleic acid

DOPC - 1,2-Dioleoyl-sn-glycero-3-phosphocholine

DPBS – Dulbecco's Phosphate Buffered Saline

EDC – 1-ethyl-3-(3-dimethylaminopropyl) carbodimide

ENP – EcoSphere™ nanoparticle

EPR – enhanced permeability and retention

FITC – fluorescein isothiocyanate

HEPES – 4-(2-hydroxyethyl)-1-piperazineethanesulfonic acid

IR – infrared

KBr – potassium bromide

MPB-PE – 1,2-dioleoyl-*sn*-glycero-3-phosphoethanolamine-N-[4-(p-maleimidophenyl) butyramide]

MPS – mononuclear phagocyte system

NaClO – sodium hypochlorite

NaOH – sodium hydroxide

NHS – N-hydroxysuccinimide

NMR – nuclear magnetic resonance

PAGE – polyacrylamide gel electrophoresis

PALS – phase analysis light scattering

PEG – polyethylene glycol

SELEX – systemic evolution of ligands by exponential enrichment

SNPs – starch nanoparticles

TEMED – tetramethylethylenediamine

TEMPO – (2,2,6,6,-tetramethylpiperidin-1-yl) oxy

Chapter 1. Introduction

1.1 Cancer

A tumor is a mass accumulation of abnormal tissue growth. [1] According to World Cancer Report 2014, cancer related deaths exceeded eight million counts world-wide in 2012, and majority of these deaths were caused by metastatic cancers. [2] The previous report published in 2008 also indicated that cancers accounted for over 12% of all deaths each year and is currently the leading cause of death in the developed countries and the second leading cause of death in the developing countries. [3] Cancer does not only threaten the well-being of individuals, it also has tremendous negative economic impact. In United States alone, more than $100 billion were spent annually on direct medical costs with another $123 billion lost due to loss of productivity. [4] It is obvious that cancer is a major global problem. With such extensive repercussions, large amounts of resources were invested to fight cancer. It is true that the overall cancer mortality rate has declined over the past few decades (Fig.1), but unfortunately, the incident rate is still on the rise. [4] Research has attributed the alarming, increasing trend largely to the aging of the population. Adaptation of unhealthy lifestyles such as smoking, alcohol consumption, poor diet, and the lack of physical activity further increase the burden. [5]

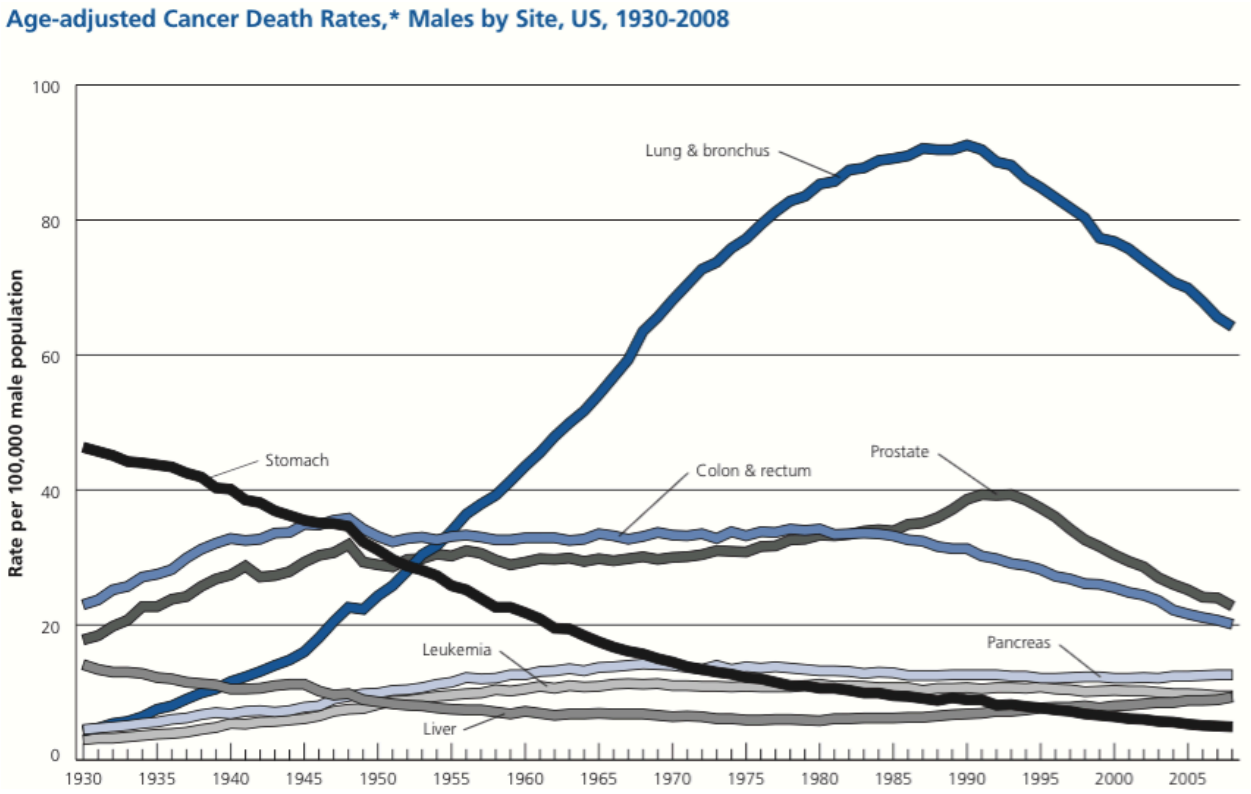

Fig. 1 - Cancer death rate in the US, 1930-2008. This figure is adapted from ref. [4]

1.2 Cancer Therapy

It is obvious that humanity has long been baffled by cancer as the famous Greek physician Galen once described cancer to be incurable. To this day, surgery remains one of the most effective treatments against cancer. Ideally, complete excision of the cancer cells by surgery would cure the disease. However, surgery alone is often inadequate due to microscopic metastasis. Furthermore, depending on patient's physical condition, surgical procedures may sometimes cause more harm than benefit. Therefore, less invasive methods such as radiation therapy and chemotherapy are often applied in conjunction with surgical procedures. [6]

When X-Ray was first discovered in 1896 by Roentgen, its unique imaging property provided the medical community with a brand new diagnostic tool. [7] Soon after X-Ray became widely available, researchers started to notice inflammation and minor tissue damage after prolonged exposures. Researchers then began to use radiation to treat many different diseases, and one of the very first attempts for radiation therapy was against cancer. [8] Radiation therapy works by damaging the genetic DNA in cancer cells through ionization; the damage can be either direct or indirect ionization. For direct ionization, the radiation directly targets the DNA molecules. On the other hand, indirect ionization targets water molecules, which then form free radicals to ionize DNA and corrupt its integrity. [9] With such vigorous mechanism of action, it is not surprising that radiation affects the cancer cells as well as the normal cells.

1.2.1 Chemotherapy

Aside from radiation therapy, the other common non-invasive treatment for cancer is chemotherapy. Chemotherapy utilizes cytotoxic chemical compounds to either destroy or restrain tumor growth. [10] Unlike surgery and radiation therapy, chemotherapy is relatively contemporary. During the First and Second World War, countries have deployed various chemical weapons on the battlefield, one of which was mustard gas. Scientists noticed that the victims exposed to mustard gas have significant reduction in white blood cell counts. They deduced that the chemical agent has the ability to target rapidly dividing cells such as white blood cells. Since uncontrolled growth is a major cancer trait, they rationalized that the chemical agent has the potential to suppress cancer cells. A compound similar to mustard gas, named nitrogen mustard was studied and found to be potent

against certain types of lymphoma. [11] Nitrogen mustard was the first of a group of chemotherapeutics called alkylating agents. Alkylating agents work by alkylating one strand of DNA or crosslinking two strands of DNA (Fig. 2). The formation of covalent bonds prevents DNA from replication, transcription, and will eventually lead to cell apoptosis. [12] Aside from alkylating agents, there are four other main classes of chemotherapeutics, namely antimetabolites, cytotoxic antibiotics, mitotic inhibitors, and topoisomerase inhibitors. [13] Each of these classes attacks cancer cells with a different mechanism. Some mimic DNA building blocks (Fig. 3), some target DNA directly, while others interfere with proteins that are essential for cellular replication. [14] As diverse as chemotherapeutics may be, they do share some similarities. For instance, most of the compounds target constantly dividing cells. [15]; therefore, hair follicles and digestive tract lining cells are usually damaged during chemotherapy, leading to the common side effects often associated with the treatment such as hair loss and loss of appetite.

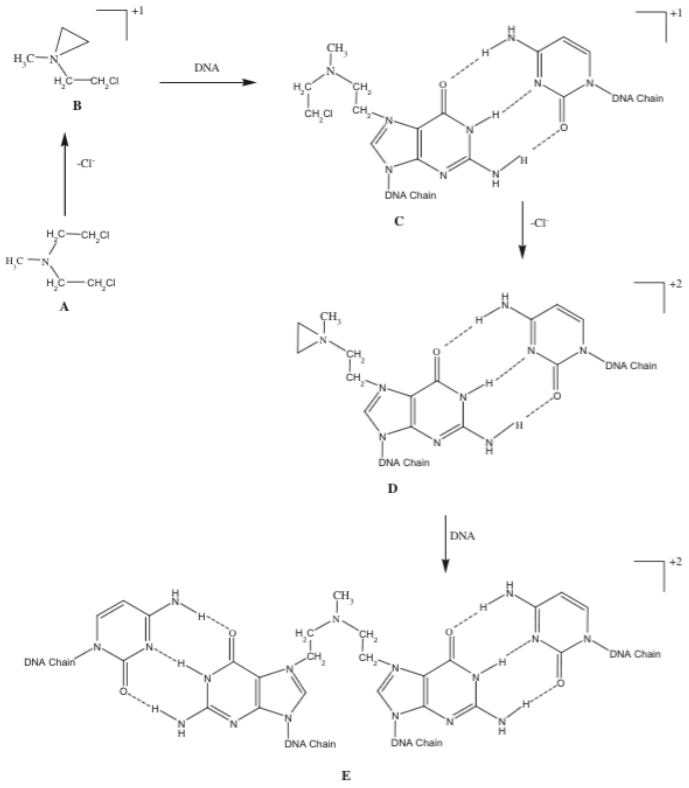

Fig. 2 – DNA alkylating agent mechanism of action. This figure is adapted from ref. [16].

The major advantage of chemotherapy is that drug molecules are small and they are distributed throughout the vascular system. Therefore, unlike surgery and radiation therapy where the treatments are localized, chemotherapy is highly dispersed and more effective against microscopic metastasis. However, the high penetrating ability acts like a double-edged sword. Cytotoxic drug molecules can reach cancer cells as well as other normal cells. Since cytotoxicity is non-discriminatory, chemotherapy often causes many adverse effects. [17] To alleviate chemotherapeutics' non-specific targeting ability, a new modality of treatment called targeted therapy has gained much attention. Targeted therapy utilizes drugs or other substances such as antibodies to identify and attack specific types of

cancer cells. [18] With the ability to distinguish cancer cells from normal cells, targeted therapy is expected to be more effective and less harmful to non-targeted cells. One example of targeted therapy is called antibody-drug conjugates (ADCs). ADCs are made of three major components, a targeting antibody, a chemically stable linker, and an anti-cancer drug. [19] The antibody will guide ADCs toward specific tumor marker and will then trigger internalization of the drug complex. After internalization, the cytotoxic drug is then released and kills cancer cells. With two ADCs already available on the market and more than thirty under clinical trial, it is not hard to see that selectivity will play a crucial role in the future of molecular anti-cancer medicine. [20]

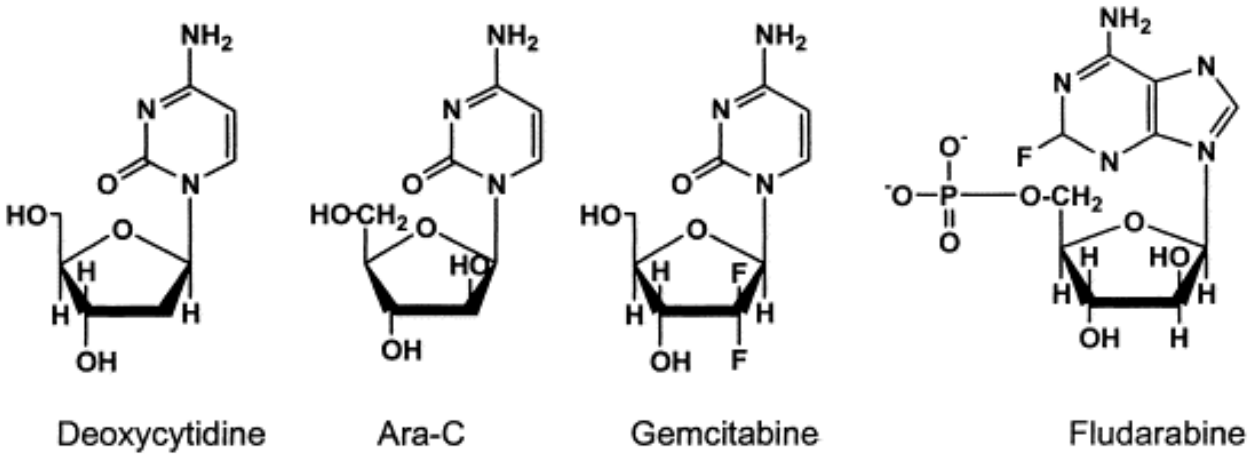

Fig. 3 - Antimetabolites mimicking DNA building block nucleotide. This figure is adapted from ref. [21]. Copyright 2000, Elsevier B.V.

1.3 Targeted Drug Delivery

Drug delivery is the process of administering pharmaceutical agents into the body to achieve therapeutic effects. Studies have shown that sustained and controlled release of

therapeutics can not only greatly enhance their efficacy, but also reduce non-specific cytotoxicity. [22] Recently, pharmaceutical companies are starting to emphasize innovating new delivery technology. Compared to the cost of developing a new therapeutic molecule, improving the efficacy of the existing drug serves as a more economical alternative.

Among these developments, a specific category called targeted drug delivery has been the center of research. [23] The concept of targeted drug delivery is to increase the therapeutic concentration exclusively at select part of the body. The selectivity and localization restricts drugs from accessing non-targeted normal cells, and thus minimizes toxic effects. [24,25] It is important to note here that targeted drug delivery is not to be confused with targeted therapy. For targeted therapy, the drugs themselves can target specific molecular markers, whereas for targeted delivery, the bioactive drugs possess no specificity. Instead, the payloads are contained within the specially engineered vehicles and the vehicles are selective.

Another important aspect for targeted delivery is prolonging the circulation time in the blood stream by avoiding the mononuclear phagocyte system (MPS) clearance. The MPS consists of the phagocytic cells such as monocytes and macrophages, and is part of the immune system. [26] The primary function of the MPS is to destroy harmful microorganisms and foreign substances. Studies have shown that the phagocytic cells in the spleen and liver can rapidly retain the majority of the administered agents. [27] Since the clearance process is mostly dependent on vehicle size and surface property, to evade this uptake, an ideal vehicle should be less than 100nm in size and should have a slightly hydrophilic surface. [28] With a longer circulation time, the vehicles have a higher ability to target the site of interest.

1.3.1 Targeting Method

There are two main types of targeting methods, passive targeting and active targeting. Passive targeting refers to the accumulation of drugs at a particular site. An example of passive targeting is the enhanced permeability and retention (EPR) effect. [29,30] The EPR effect refers to the phenomenon that molecules in the nanometer range have a tendency to accumulate near cancerous tissues rather than normal tissues. As mentioned previously, one of the hallmarks of cancer is continuous angiogenesis to support the rapid tumor expansion. This irregular angiogenesis results in defective local vasculatures that are leaky to particles below a certain size. [31] (Fig. 4). The EPR effect is critical important for a delivery system designed to target cancer.

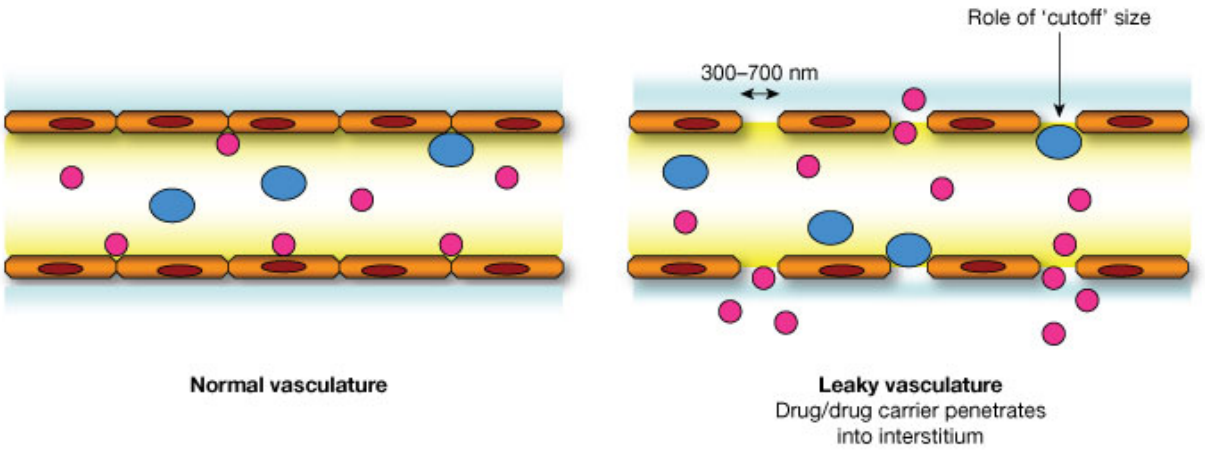

Fig. 4 – Enhanced permeability and retention effect. This figure is adapted from ref. [32]. Copyright 2010, SAGE Publications.

As for active targeting, the delivery system is modified with active agents having selective affinity towards biomarkers. [33-35] Active targeting can be further classified into three different levels. First order targeting, or organ targeting, is when the delivery system releases the payload in a specific organ. Second order targeting, or cellular targeting, is when the drug is released to the particular tissues or cells. Lastly, third order targeting, or subcellular targeting, is when the system can deliver the drug to the intracellular site of the specific cells. [36] With increasing order, targeting specificity increases as well as the level of sophistication needed. Ideally, an anti-cancer targeting vehicle should achieve cellular targeting, if not subcellular targeting. The active agents responsible for targeting are called homing devices. These homing devices are often part of a pair of molecules that have a strong affinity for each other. Interactions such as lectin–carbohydrate, ligand-receptor, and antigen-antibody are most commonly used. [37]

Other than the homing devices mentioned previously, there is another type of molecules called aptamers that have attracted much attention in the past 25 years and is praised as the future of affinity molecules. [38] Aptamers are pieces of oligonucleotides obtained through systematic evolution of ligands by exponential enrichment (SELEX) process (Fig. 5). SELEX is a technique for producing single-stranded oligonucleotides with affinity toward a specific ligand. In a typical SELEX cycle, an initial oligonucleotide library is generated with fixed-length random region flanked by conserved 3’ and 5’ ends. The random sequences are exposed to the target ligand and the ones that do not bind to the target are removed. Binding sequences are then eluted and amplified for subsequent rounds of selection. After approximately ten to fifteen cycles, the remaining sequences are cloned and sequenced. Prior to aptamers, antibodies have been the gold standard of affinity

agents. However, its large size and instability has always been a major drawback. Aptamers' reputation stemmed from their strong affinities comparable to that of antibodies. Since aptamers are oligonucleotides, they can withstand a much harsher temperature and pH than antibodies do. [39,40] Unlike antibody production, aptamers are chemically synthesized and thus have miniscule batch-to-batch difference. With so many improvements and great flexibility for modification and coupling, countless studies have been done using aptamers as the homing agents. [41-43]

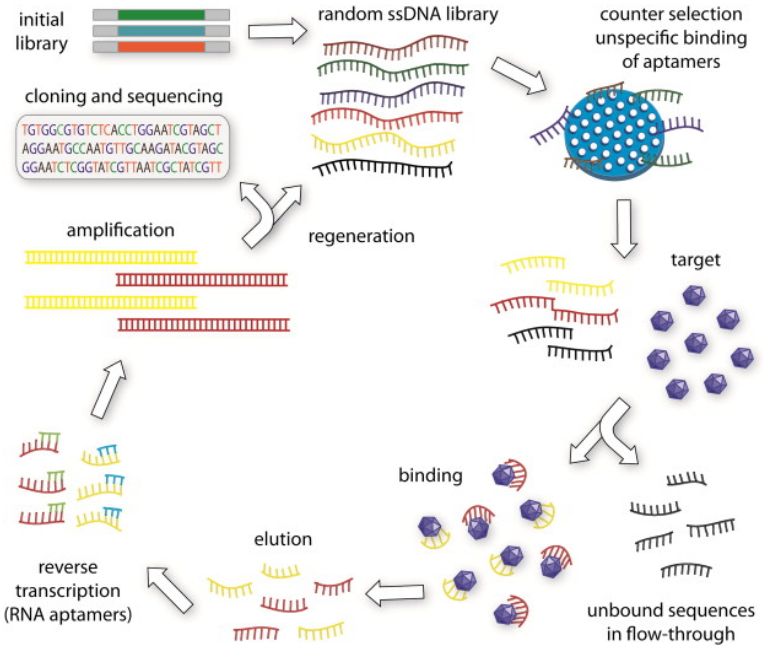

Fig. 5 – The SELEX system cycle. This figure is adapted from ref. [44]. Copyright 2015, Elsevier B.V.

1.4 Nanoparticle Delivery System

Designing a delivery system involves many complications such as toxicity, stability, biocompatibility, biodegradability, and cost effectiveness. [45] To take it one step further, a

targeted delivery system is even more complex and requires higher sophistication. On top of all the requirements, an ideal targeted delivery system also needs to restrict drug distribution to only the target location. In terms of anti-cancer targeted delivery system, one of the most actively researched topics is nanoparticles. As a targeted delivery system, nanoparticles possess many unique advantages. For starters, nanoparticles in the size range of 10-100nm can simultaneously take advantage of the EPR effect and avoid renal clearance. [46] By fine-tuning their surface properties, nanoparticles can avoid macrophage uptake and have high tumor penetration. Nanoparticles' high surface area is also capable of accommodating multiple targeting agents, which can allow multi-valent binding to further increase affinity. [47] Lastly, nanoparticles have a large payload capacity, capable of carrying multiple types of drugs and can protect therapeutics from potential degradation. [48]

With more than ten commercialized drugs on the market, liposome-based systems are currently the most common nanoparticle delivery system. [49,50] Liposomes are synthetic vesicles composed of at least one lipid bilayer. Liposome's success can be attributed to its attractive biological properties such as high biocompatibility and low toxicity. Its surface property and size can be easily manipulated. And most importantly, liposomes are capable of accommodating both hydrophilic and hydrophobic drugs. [51] Clinical studies have shown improved efficacy and reduced cytotoxicity for liposome-enclosed chemotherapeutics such as doxorubicin. [52] However, one major flaw for liposomes is its susceptibility to MPS clearance and therefore short circulation time. [53] A number of solutions have been proposed including masking the particle with polyethylene glycol (PEG). [54] Apart from liposome systems, the FDA also approved a few other types of nanoparticles such as protein nanoparticles and polymeric micelles. [55,56] Each type of nanoparticles has their

own unique strengths and weaknesses, and recently more attention are started to focus on using biodegradable materials for drug delivery.

1.5 Structure and Chemistry of Starch

Before any further discussion about biodegradable nanoparticles, it is important to take an in-depth look into starch, as it is the material of choice for this thesis. Starch is synthesized by most plants as energy storage, and is one of the most abundant materials on Earth. As a biodegradable, non-toxic, and cheap biopolymer, starch has a wide spectrum of applications. Pharmaceutical companies use starch as drug tablet filler; food companies use starch film as barrier for packaging; and paper companies uses cooked starch as coating for desirable properties. [57] Extensive research has been done to analyse starch's composition and structure but it is only until the last decade do we have a more accurate concept of starch's chemistry.

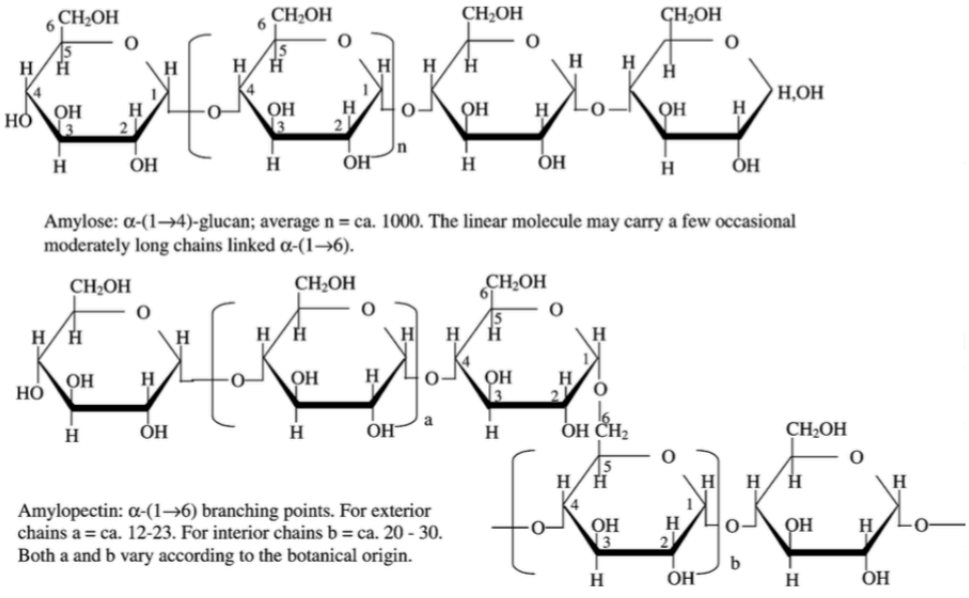

Fig. 6 – Structures of amylose and amylopectin. This figure is adapted from ref. [58].

The basic macrostructure of starch is a starch granule. A starch granule is composed of two similar macromolecules made with α-glucose building block, amylose and amylopectin (Fig. 6). Amylose is a linear polymer of glucose units connected with mostly α (1, 4) bonds and some α (1, 6) branching. Compared to amylopectin, the highly linear amylose has relatively low molecular weight of around 1 x 10^6. On the other hand, amylopectin is highly branched with one α (1, 6) branching per 22 glucose units. The heavily branched amylopectin structure has much larger molecular weight of 1 × 10^8. Starch granules from different botanical sources have different ratio of amylose to amylopectin, and therefore different characteristic. Another important property about amylose and amylopectin is that the polymeric chains can form double helices and may be partially crystalized. [59] The crystalline may be either A-type where the helices are tightly packed with less water molecules, or B-type with a more open structure and a hydrated core (Fig. 7). Recent findings also suggest a C-type structure that is a combination of both A- and B-type.

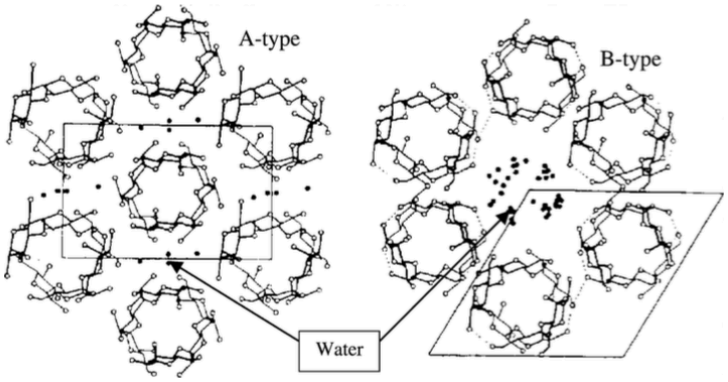

Fig. 7 – A- and B-type starch crystalline. This figure is adapted from ref. [59]. Copyright 2004, Elsevier B.V.

Due to the great complexity of starch structure, a universally accepted model is still lacking. However, one prevailing model is a multi-scale structure subdividing starch from granule to the two α-glucan. [60] (Fig. 8). Starch granule is made of alternating layers of amorphous growth rings and semicrystalline growth rings. The semicrystalline growth ring is packed with special sub-units called blocklets. Blocklets are 20~50nm in length and constitutes of alternating stacks amorphous and crystalline lamellae. The crystalline region is made of tightly packed amylopectin double helices, whereas the amorphous lamellae correspond to the branching point of amylopectin. On the other hand, amylose is randomly distributed in both the amorphous and crystalline region.

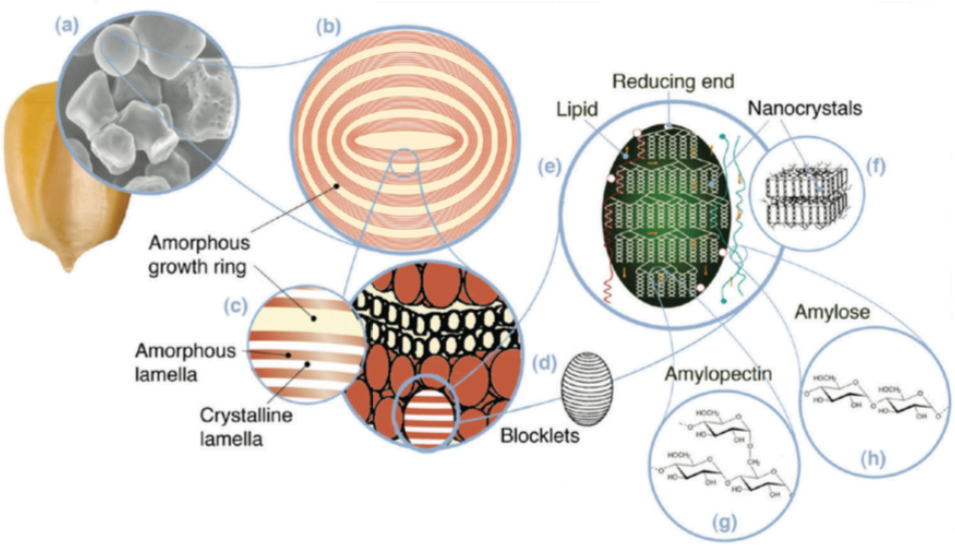

Fig. 8 – Starch multi-scale structure. This figure is adapted from ref. [61]. Copyright 2010, American Chemical Society Publications.

1.6 Polysaccharides Delivery System

Biodegradable nanoparticles are sub-micron particles typically with size below 100nm. Aside from the previously mentioned advantages of a nanoparticle delivery system, its biodegradability also provides the carrier with controlled release potential. [62] Many polymeric materials such as polylactic acid, polyglycolic acid, proteins, and polysaccharides have been explored for drug delivery application. Among these materials, polysaccharides have gained increasing attention with their outstanding properties. As natural biopolymers, polysaccharides are non-toxic and readily biodegradable. [63,64] They can be found in a variety of plants and animals with a wide range of molecular weights. [65] Polysaccharides such as cellulose, chitosan, and alginate are among the most abundant biomass. Extraction and processing of polysaccharides have relatively low cost. From a chemical perspective, polysaccharides have many reactive groups and can be easily modified for desirable properties. Furthermore, many polysaccharides have hydrophilic functional groups such as hydroxyl, amino, and carboxyl, which favour the formation of non-covalent binding with biological tissues. [65] The bio-adhesion property can often increase drug residence time.

Some of the earliest studies on polysaccharide nanoparticles were done on chitosan due to its strong bio-adhesion. Particles were first prepared through covalent crosslinking. However, subsequent studies exposed the toxicity of crosslinkers and suggested alternative crosslinking mechanisms such as ionic crosslinking with charged ions. [66] Another popular particle synthesis method is modifying polysaccharides with hydrophobic chains; so the amphiphilic copolymers can self-aggregate in aqueous conditions to form nanoparticles. Other than chitosan, cellulose is also under active research for its delivery potential. Similar to starch, cellulose is also made of glucose and contains both amorphous and crystalline

regions. A common method of preparing cellulose nanoparticles is to subject cellulose to acid hydrolysis to remove the amorphous region. [67] The resulting elongated particles specifically known as cellulose nanocrystals have proven to be non-toxic and capable of delaying MPS clearance. [67]

1.6.1 General Methods for Starch Nanoparticle Preparation

Compared to other polysaccharides, there are fewer studies on starch nanoparticles (SNPs) and their applications. [68,69] The SNP preparation methods can be classified into either a top-down or a bottom-up process. Top-down process refers to breaking down of larger starch particles such as granules or micron size starch, into nanoparticles. On the other hand, bottom-up process describes the build-up of smaller molecules into larger macromolecules. Examples of bottom-up processes are self-assembling and nano-precipitation. [70-72] Most of the current literature follows the top-down process since the starch granule is the most readily accessible starting material.

As mentioned before, starch shares similar chemical structure with cellulose and they both have crystalline and amorphous region. Therefore, just like cellulose, acid hydrolysis is one of the most common methods of preparing SNPs. [73] Studies have shown most starch hydrolysis occur in a two-stage process. The initial rapid hydrolysis stage can be attributed to the disintegration of the amorphous region. The subsequent break down of the crystalline region is significantly retarded by the densely packed helices. A milder preparation process for SNPs is enzymatic degradation. A handful of studies have recorded using α-amylase to breakdown starch into submicron fragments. [74] However, one major flaw with enzymatic treatment is that the resulting starch particles have broad a size

distribution. Aside from chemical processes, different physical treatments such as ultrasonication, extrusion, and high-pressure homogenization have also been used to breakdown starch granules into SNPs. [75,76] Since breaking down granule into nanoparticle is heavily affected by the source, pH, temperature and the amount and type of crosslinking agent, the lab scale produced starch nanoparticles often suffer from large batch-to-batche variation. In this thesis, we aim to test a starch nanoparticle that is produced in an industrial scale.

1.6.2 EcoSphere™

Currently there are only a couple of industrial applications for SNPs. EcoSphere™ produced by EcoSynthetix Inc. is one of the commercially available SNPs. EcoSphere™ is marketed as a bio-based latex in substitution of petroleum-based binder and paper coating. EcoSphere™ has been proven to have superior quality over synthetic latex and much more environmental friendly. [77] The particles are prepared through a patented reactive extrusion process capable of simultaneously extruding and crosslinking. [77,78] Starch premix and plasticizer glycerol are fed simultaneously into the twin-screw extruder. The extrusion process exposed starch to high pressure and temperature. [79] The vigorous condition destroys starch's crystalline region and completely gelatinized. With the addition of crosslinker, the α-glucan chains can be crosslinked. And by adjusting the amount of crosslinker, the resulting SNPs' size and properties can be controlled.

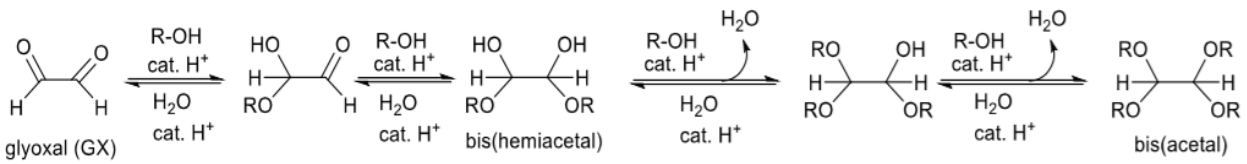

Fig. 9 – Glyoxal crosslinking mechanism, R-OH represents the hydroxyl group on glucose. [80]

The crosslinker used to prepare EcoSphere™ nanoparticles (ENPs) is glyoxal. Glyoxal can crosslink the α-glucan chains by forming either hemiacetal or acetal group with the hydroxyl on the glucose units (Fig. 9). Data suggest higher crosslinker concentration would result in smaller ENPs. Fundamental studies conducted by EcoSynthetix Inc. also observe swelling behaviour when ENPs are dispersed in an aqueous solvent (Fig. 10). This unique property is favourable for drug delivery since previous studies suggest that the drug loading efficiency is correlated to the degree of swelling. [81]

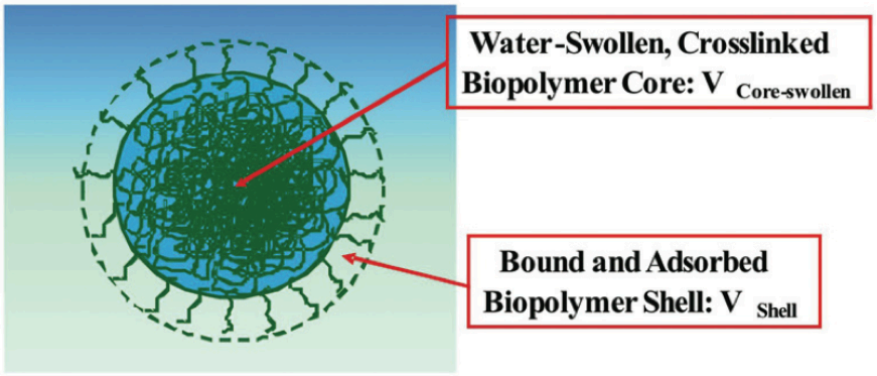

Fig. 10 – EcoSphere™ nanoparticle swollen structure. This figure is adapted from ref. [81]. Copyright 2004, Elsevier B.V.

1.7 Thesis Objective

The objective of this research is to develop an ENP-based drug delivery vehicle, specifically for anti-cancer purposes. As a starch-based material, EcoSphere™ has high biocompatibility, good biodegradability, and is cheap to produce. Furthermore, as a nanoparticle of size below 100 nm, EcoSphere™ takes advantage of the EPR effect and facilitates local accumulation in tumors. Therefore, ENPs serve as an excellent platform for anti-cancer drug delivery. To further strengthen ENPs' capabilities, a homing device will be modified onto the nanoparticles. To be more specific, aptamers will be used to guide the vehicle toward targeting the right cells. The modification strategy involves two main steps, oxidation and aptamer conjugation (Fig. 11). ENPs will be first subject to (2,2,6,6,-tetramethylpiperidin-1-yl)oxy (TEMPO)-mediated oxidation to convert its C6 hydroxyl group into carboxylic group. After partial oxidation, amine-modified aptamers are conjugated onto the nanoparticles through 1-ethyl-3-(3-dimethylaminopropyl) carbodimide (EDC) and N-hydroxysuccinimide (NHS) coupling. After the modifications, the resulting vehicle properties such as cellular internalization and selectivity are to be evaluated and compared against market available delivery vehicle.

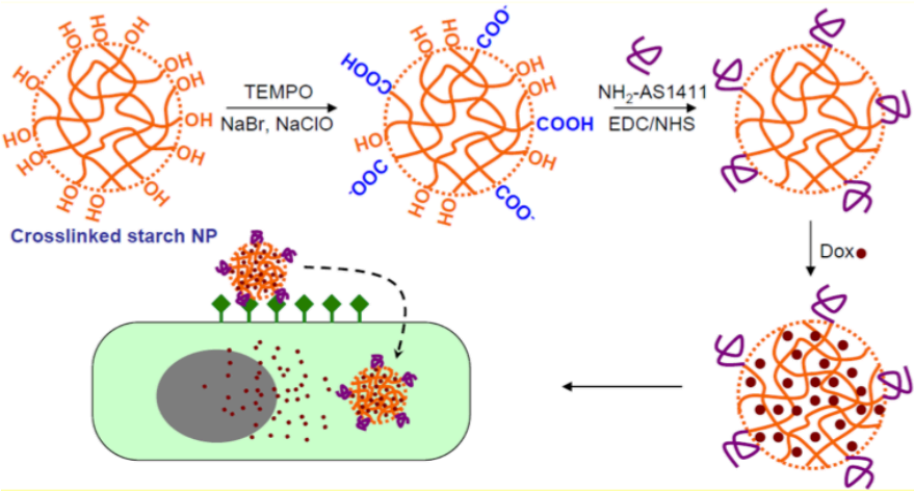

Fig. 11 – Schematic for ENPs modification. [82]

The two modification processes and the final evaluation study constituted the three major milestones of this thesis, and therefore one chapter will be dedicated to each milestone. For oxidation, ENPs are subject to different levels of oxidation and characterized with spectroscopic techniques. For aptamer conjugation, gel electrophoresis will be used to quantify coupling efficiency. The conjugation process is also subject to optimization to reduce DNA loss. Finally, the modified vehicle will be evaluated using microscopy and be compared to market available liposomes.

Chapter 2. Oxidation of Starch Nanoparticles

Starch is a polymer made of glucose. To attach DNA to starch nanoparticles, the first step of modification is to selectively oxidize starch's C6 hydroxyl group to carboxyl group. Since the hydroxyl moiety is less reactive, oxidizing it to a carboxylic group is required for the subsequent coupling reaction. ENPs provided by EcoSynthetix Inc. are subject to a different extent of oxidation to evaluate the optimal oxidation level for the subsequent conjugation. To confirm oxidation process, spectroscopic measurements such as nuclear magnetic resonance (NMR) spectra were collected. Particle colloidal properties such as size and ζ-potential were also measured using dynamic light scattering (DLS) and phase analysis light scattering (PALS).

2.1 TEMPO Oxidation of ENPs

TEMPO-mediated is a racial catalyst used for oxidizing primary alcohols. Multiple studies have shown TEMPO-mediated reaction on different polysaccharides resulting in highly selective primary hydroxyl oxidation. [83,84] In the case of starch, only the C6 hydroxyl is converted. The complete TEMPO-mediated oxidation is a two-step process (Fig.12). The primary alcohol is oxidized into an aldehyde before a second oxidation into a carboxyl group. As shown in the reaction mechanism, the initial hydroxyl is oxidized by TEMPO. The other catalyst, hypobromite helps to reactivate TEMPO for further reactions. The addition of sodium hypochlorite then restores hypobromite's catalytic activity. For the second oxidation to occur, the resulting aldehyde first forms an intermediate with hydroxide ions before further oxidation. To completely oxidize one mole of hydroxyl into carboxyl, two moles of sodium hypochlorite (NaClO) and one mole of sodium hydroxide

(NaOH) are needed. Therefore by calculating the number of C6 hydroxyl and adjusting the amount of NaOH added, oxidation extent can be controlled. Since the optimal reaction is at pH 10-11, reaction pH is also monitored. [85]

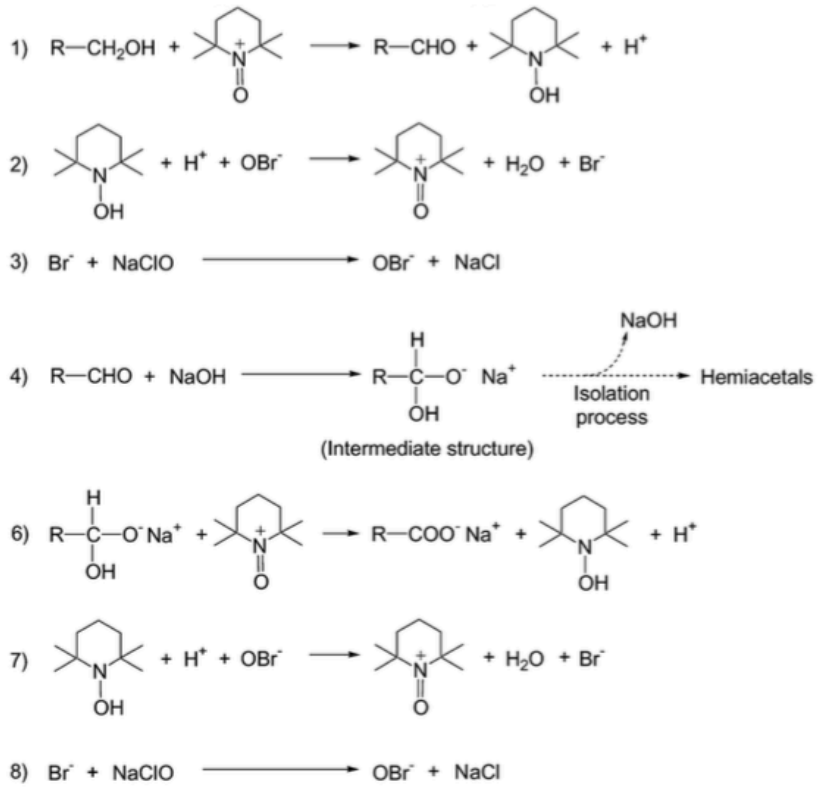

Fig. 12 – TEMPO-mediated oxidation mechanism. This figure is adapted from ref. [83].

ENPs obtained from EcoSynthetix Inc. were subject to TEMPO-mediated oxidation at 1%, 2%, 5%, 10% and 20%. Dextrin is the product of starch hydrolysis, and was used as the experimental control and oxidized to 2% and 20%. After oxidation, starch was precipitated with excess ethanol and lyophilized to obtain powered product. Prior to any characterization, an evidence of oxidation can be observed from sample's solubility in

water. Figure 13 shows 40 µL of 5% (w/w) oxidized starch and dextrin samples precipitated with excess ethanol. The samples were oxidized to different extents and it is obvious that samples with a higher oxidation level are less susceptible to precipitation. The oxidation process introduced hydrophilic carboxyl groups to starch. Therefore compared to the others, the more oxidized samples have a higher solubility in water and is thus more easily dispersed.

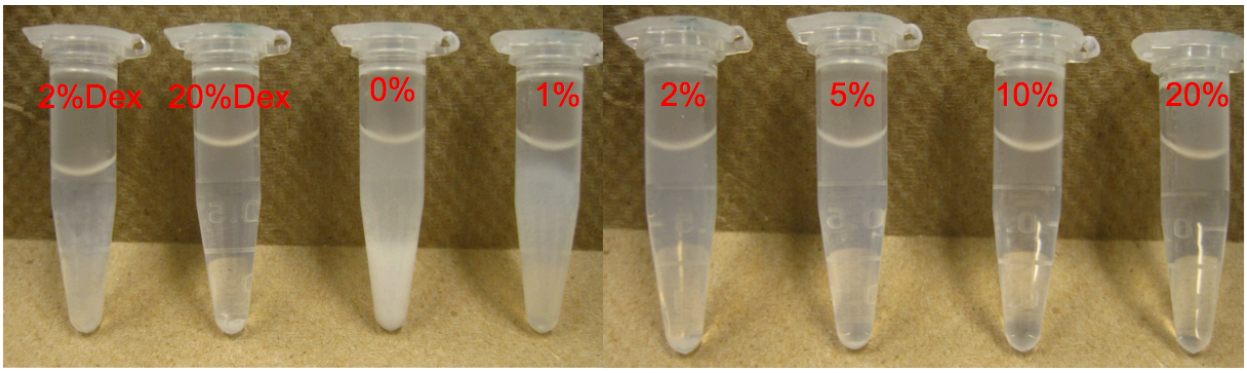

Fig. 13 – Oxidation level V.S. starch solubility in water.

2.2 Spectroscopic Characterization

To further confirm ENPs' oxidation, spectroscopic measurements were used.

2.2.1 NMR

For non-oxidized starch, all the hydrogen are attached to aliphatic carbon or hydroxyl, therefore, shifts on proton NMR should all be below 6 ppm. And as previously mentioned, TEMPO-mediated oxidation can produce either a carboxylic group or an aldehyde group. An easy indication for oxidation is the presence of shifts at around 9 ppm for the aldehyde proton. Similar logic can be applied to the ^{13}C NMR. Non-oxidized starch has exclusively

alkane carbon and therefore all shifts should be below 120 ppm. [86] Any signal above 160 ppm represents the carbonyl from either carboxyl or aldehyde. For quantitative analysis, integration of aldehyde shift on ^{1}H NMR can be compared with the non-oxidized C6 shift. On ^{13}C NMR, integration of both carbonyl shifts from aldehyde and carboxyl can also express the relative oxidation extent.

For cleaner spectrums, the NMRs of the oxidized ENP samples were done in D_2O. Therefore the exchangeable proton on carboxyl cannot be observed. What is observable is the other oxidation product, aldehyde. As shown in Fig. 14, oxidation can be confirmed with the aldehyde proton peak at around 9.1 ppm displaying increasing intensity with increasing oxidation level. The observed shift intensity does not increase linearly with the oxidation extent. This non-linear correlation is due to the two-step oxidation mechanism. Initially, oxidation will produce mostly aldehyde and much less carboxyl, but as oxidation continues, more and more of the aldehyde will be converted into carboxyl. Therefore, the intensity of the aldehyde shift at 9 ppm will first increases, then plateau and eventually disappears as the oxidation level increases. Interestingly, there are also minor unidentified shifts under 6ppm showing proportional strength with increasing oxidation level.

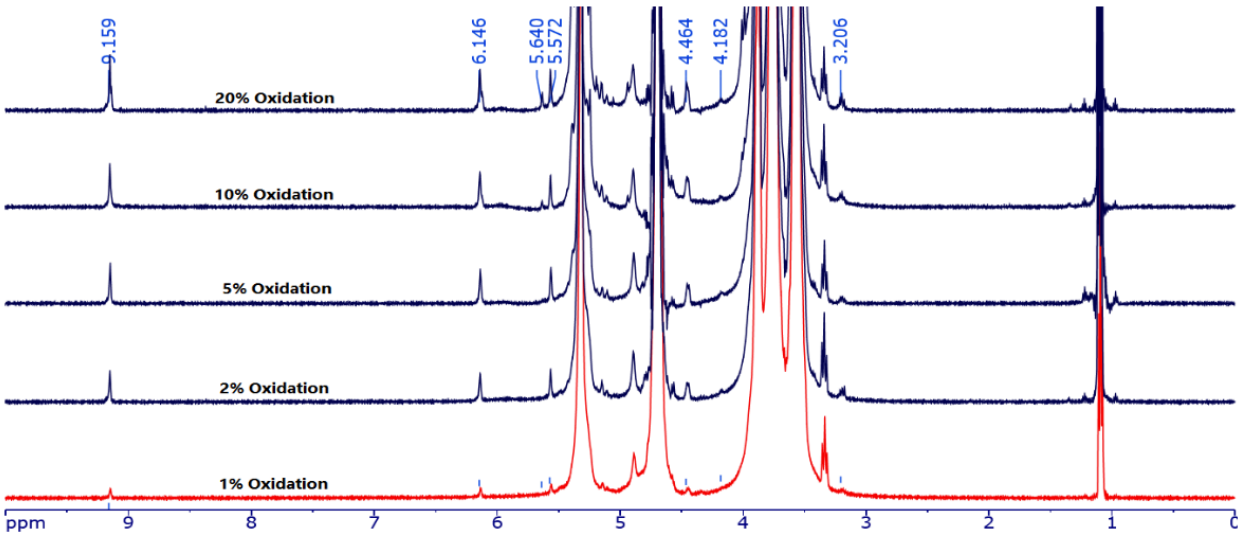

Fig. 14 – ^{1}H NMR spectrums of oxidized ENP samples.

^{13}C NMR was also done to directly observe carboxyl groups. Since ^{13}C NMR is not as sensitive as ^{1}H NMR and the carbonyl group is only present in a small amount, only the 20% oxidized ENP sample was measured. The measurement was left over night to obtain maximum signal strength. As shown in Fig. 15, the majority of the shifts are below 120 ppm and belongs to the non-oxidized starch. The two signals observed at around 190 ppm and 175 ppm were identified to be the aldehyde and the carboxyl carbon respectively. Due to the low signal to noise ratio, shift integration and quantitative analysis were not done. However, the relative strength of the two carbonyl shifts and the ratio of carbonyl shifts to non-oxidized C6 shifts were in close agreement with the literature. [80]

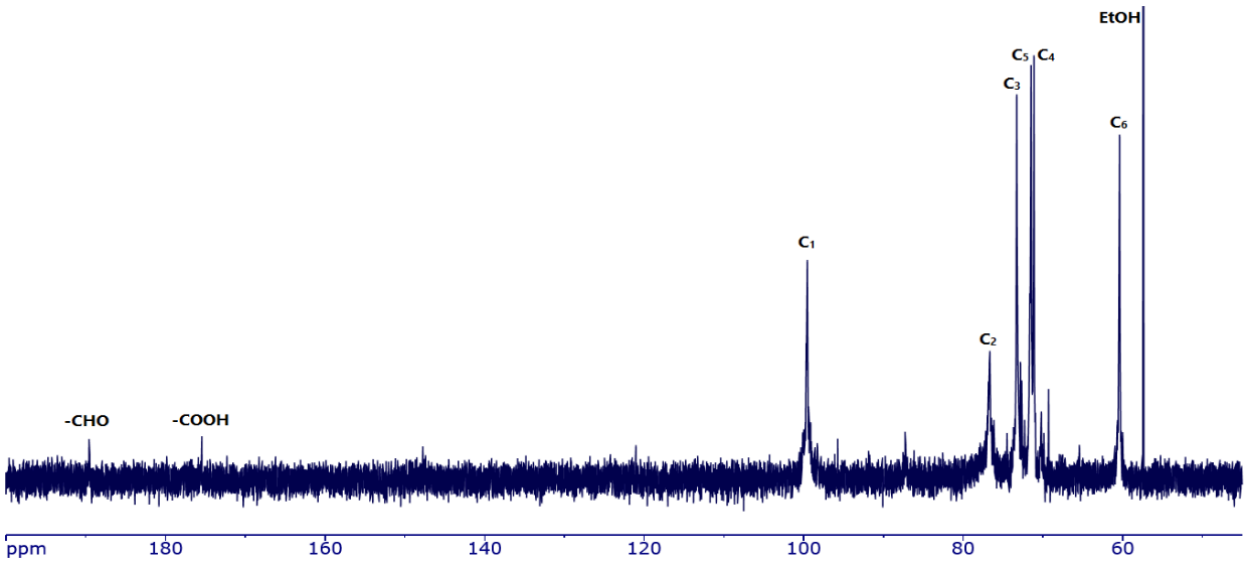

Fig. 15 – ^{13}C NMR spectrum of 20% oxidized ENPs.

2.2.2 DLS and Zeta-Potential

The oxidized ENP size and ζ-potential were measured using DLS and PALS respectively at three different pHs. Previous literatures indicate that unmodified ENPs are under 50 nm and no net charge on particle surface. Since TEMPO-mediated oxidation was done at pH 10-11, some depolymerisation on starch chains are expected. Furthermore, after oxidation, carboxylic groups are introduced onto the particles, and therefore the surface charge will most likely be affected.

For the DLS measurements, the non-oxidized ENP sample size stayed relatively stable at just under 30 nm for all three pHs (Fig. 16). The less oxidized samples, namely the 1%, 2%, and 5% showed slight size reduction but consistent throughout the three different pHs. The decreasing size can be attributed to the α-1,6-glucosidic bond cleavage during the oxidation process. For the 10% and 20% oxidized samples, a significant increase in size was observed especially at pH 7 and 8. Size measurements also increased at pH 9 but not as

significant. The size increase for more oxidized samples is counterintuitive since depolymerisation were expected during oxidation. One possible explanation for the size increase is hydrogen bonding. We noticed bulk gel formation when the oxidized ENPs were heated. The gelation observed was reversible by changing the oxidized ENPs concentration in water. After partial oxidation, starch chains acquire carbonyl groups from either aldehyde or carboxyl. The newly introduced carbonyls can interact with adjacent hydroxyls to form hydrogen bonds and possibly lead to aggregation. Small starch fragments from depolymerisation may also contribute to aggregation by exposing more surface area for hydrogen bonding.

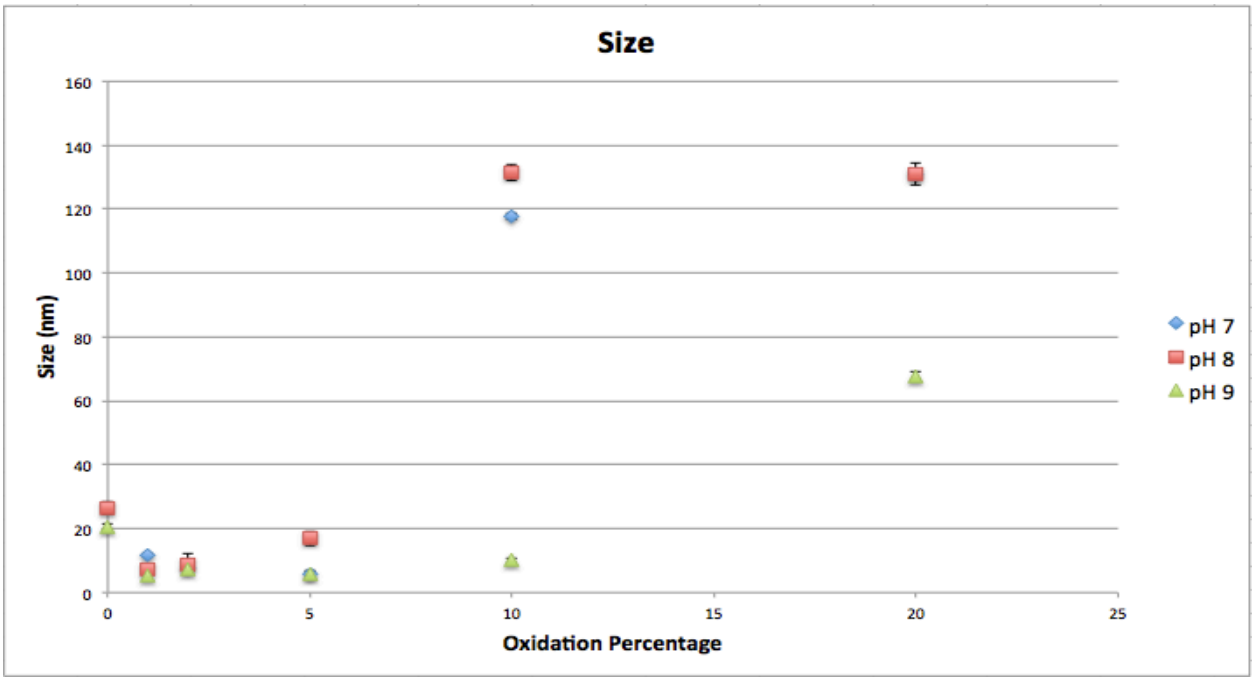

Fig. 16 – Size measurements of oxidized ENP samples at different pHs. The ENP concentration was 1% (w/w).

The ζ-potential of the oxidized ENPs was measured using PALS. PALS measures particle ζ-potential by applying an electric field to the dispersion. The particles then move with a velocity related to their charge and the velocity is measured to calculate its ζ-potential. For ζ-potential measurements, the non-oxidized ENPs have charge close to 0 mV. This result is in close agreement with previous findings. [87] For the different oxidized samples, as the oxidation levels increase, the particle surface charge displays a decreasing trend. This phenomenon is intuitive as oxidation introduces negative carboxyl groups to starch chains, resulting in higher oxidation and more negative charges.

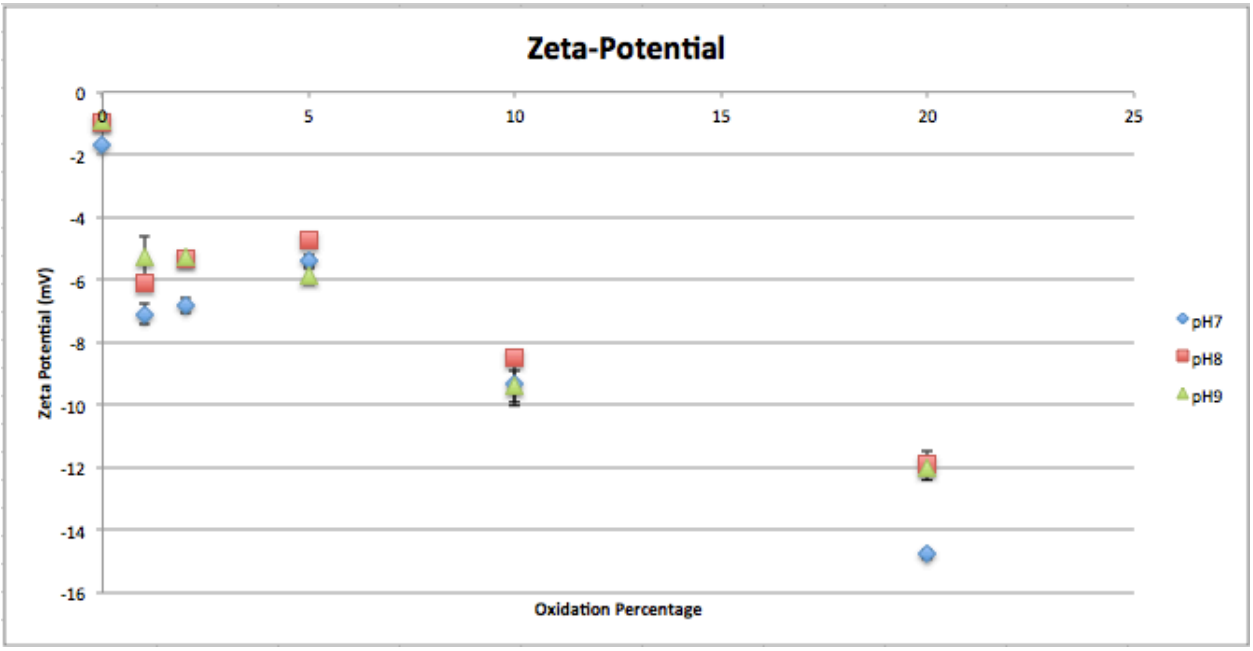

Fig. 17 – ζ-potential measurements of oxidized ENP samples at different pHs. The ENP concentration was 1% (w/w).

2.3 Materials and Methods

2.3.1 Materials

ENPs with different crosslinker densities were provided by EcoSynthetix Inc. (Burlington, ON). To avoid potential crosslinker toxicity, a specific batch of ENPs with 0% crosslinker coded GX0 were used in this study. TEMPO, NaBr, KBr, NaClO and ethanol were purchased from Sigma Aldrich (St. Louis, MO). NaOH was purchased from Mandel Scientific (Guelph, ON). All chemicals were used without further purification. All aqueous solutions were prepared using Milli-Q water (18.2MΩ resistivity).

2.3.2 TEMPO-mediated Oxidation of SNP

The TEMPO-mediated oxidation of ENPs followed the protocol described by Kato et al. 2 g of GX0 ENPs were dispersed in 50 mL of Milli-Q water at 5% (w/w). The starch solution was kept at 4 °C using an ice bath. 317.5 mg of NaBr and 24 mg of TEMPO were dissolved individually with 50 mL of Milli-Q water. Both NaBr and TEMPO solution was added into starch solution and the pH of the mixture was adjusted to 10.75 with NaOH. Reaction was initiated by the added aliquot of 5% NaClO into the mixture. Aliquots of 0.5M NaOH were constantly added to maintain reaction at pH10.75. After the desired oxidation level was achieved, excess ethanol was added into the reaction mixture to precipitate starch. The mixture was kept on ice to allow precipitation for 30 minutes before being centrifuged at 7800 rpm for 20 minutes. The supernatant was discarded and the pellets were re-dispersed in 50 mL of Milli-Q water. The ethanol precipitation and centrifugation was repeated again before the pellets were lyophilized overnight to obtain the powdered product.

2.3.3 Spectroscopic Characterization

NMR

70 mg of oxidized ENPs were dispersed in 700 μL of D_2O for 2 h. Both ^{1}H and ^{13}C spectrum were obtained using 300MHz Bruker Avance 6-Channel NMR spectrometer.

DLS and PALS

Oxidized ENP samples were dispersed and diluted to 1% (w/w) using 10 mM pH 7.4 4-(2-hydroxylethyl)-1- piperazineethanesulfonic acid (HEPES) buffer. Measurements for both particle size and ζ-potential were done using Malvern Zetasizer.

`

Chapter 3. DNA Conjugation

The second part of ENP modification is to conjugate aptamers onto the oxidized particles for active targeting. Oxidized ENPs from the previous modification are now capable of conjugating with amine-modified molecules using the EDC/NHS coupling chemistry. The first objective is to determine the optimal oxidation level from the various samples. Amine-modified dye molecules and control oligonucleotides were conjugated to evaluate coupling efficiency. To better visualize and quantify conjugation, conjugated products are subject to gel electrophoresis. And since aptamers are expensive, the last part of the process focuses on optimizing aptamer conjugation efficiency. Various reaction parameters and synthesis process are investigated to minimize DNA loss.

3.1 EDC/NHS-Mediated Aptamer Conjugation

Zero-length linkage refers to direct covalent bond linking an atom of one molecule to the other molecule without any linkers or spacers. The presence of linker may affect the affinity of targeting agent, and thus using zero-length linkage minimizes potential complications. [88] EDC is a water-soluble carbodiimide, widely used for conjugating biological substances containing amine and carboxyl groups. EDC can react with carboxyl to form a reactive but unstable isourea intermediate, and the intermediate is susceptible to nucleophilic attack from primary amines to form an amide bond. However, EDC is used in aqueous environment, and water often acts as a nucleophile to hydrolyze the intermediate. Therefore, the reaction in aqueous conditions often suffers from low yield. [89] To improve reaction yield, it is very common to add NHS during EDC coupling process. Similar to the

EDC mechanism, the carboxyl group first forms the unstable intermediate with EDC. Then the carboxylic is transferred onto NHS forming a more stable ester bond (Fig. 18). The ester intermediate is less susceptible to hydrolysis, but acts as a great leaving group in the presence of primary amines. The products of either reaction are identical, but NHS facilitates process produced significantly higher yield.

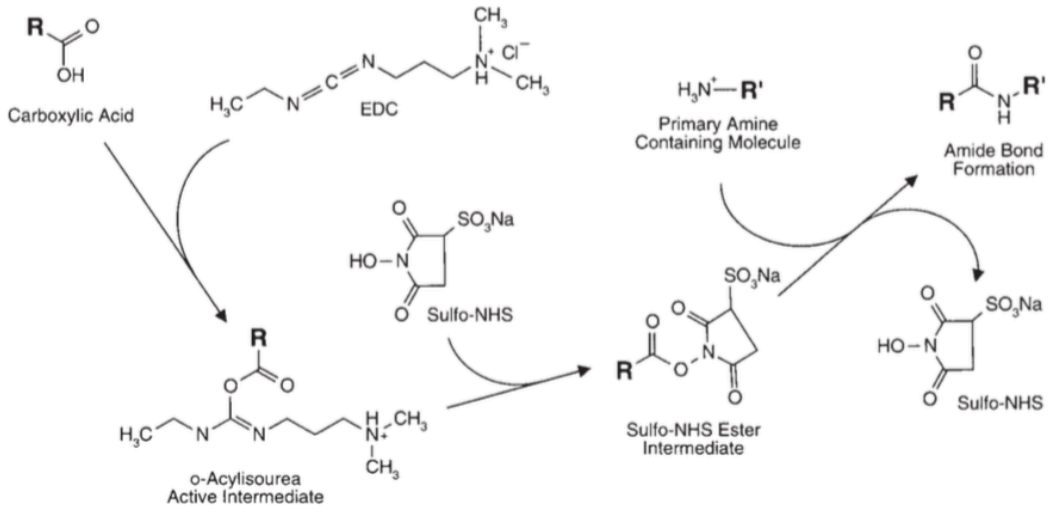

Fig. 18 – EDC/NHS conjugation mechanism. This figure is adapted from ref. [90].

All the samples from previous oxidation steps were first subject to EDC/NHS coupling with amine-modified dye molecules. The samples were also conjugated with amine and dye dual-modified control DNA fragment (Cy3-T15-NH_2). Denaturing polyacrylamide gel electrophoresis (PAGE) was used to evaluate the conjugation efficiency of each sample.

3.1.1 Gel Electrophoresis Based Characterization

Polyacrylamide gel electrophoresis is a technique widely used in biochemistry and molecular biology to separate biological macromolecules like proteins and nucleic acids. Molecules may be run in their native form to preserve their higher order structure or in a denatured form whose mobility is only dependent on molecule size and mass to charge ratio. [91] Since our objective of running gels is to quantify conjugation efficiency, there is no need to preserve DNA structure and therefore samples were denatured with urea and subject to denaturing PAGE.

The first conjugation attempt was between oxidized ENPs and an amine-modified dye molecule named HiLyte Fluor 488. Conjugated samples were diluted appropriately and mixed with denaturant urea before loading into the gel. As shown in denaturing PAGE result, the first lane serves as the negative control with just the dye molecules and no ENPs (Fig. 19). Although the detailed structure of dye molecules is unknown, seeing that the molecule migrated toward the cathode end, it is safe to assume that the molecule is negatively charged. The next two lanes are oxidized dextrin serving as the positive control. The most obvious contrast between the two samples is the difference in fluorescent intensity. The 2% oxidized dextrin has significantly lower intensity than the 20% sample. This difference in fluorescent intensity can also be observed in the oxidized ENP samples. The intensity seems to be proportional to the oxidation extent with the 20% sample showing the highest intensity and non-oxidized sample showing no fluorescence at all. This result suggests either higher oxidation levels are favourable for coupling process or the high fluorescence simply comes from more conjugation sites. Another interesting

observation is the speed of band migration. ENPs are significantly larger than dye molecules, and are expected to be trapped by the gel without much migration. However, smeared bands suggesting a broad size distribution was observed with the higher oxidation samples. This result hints at possible degradation of ENPs during the oxidation process.

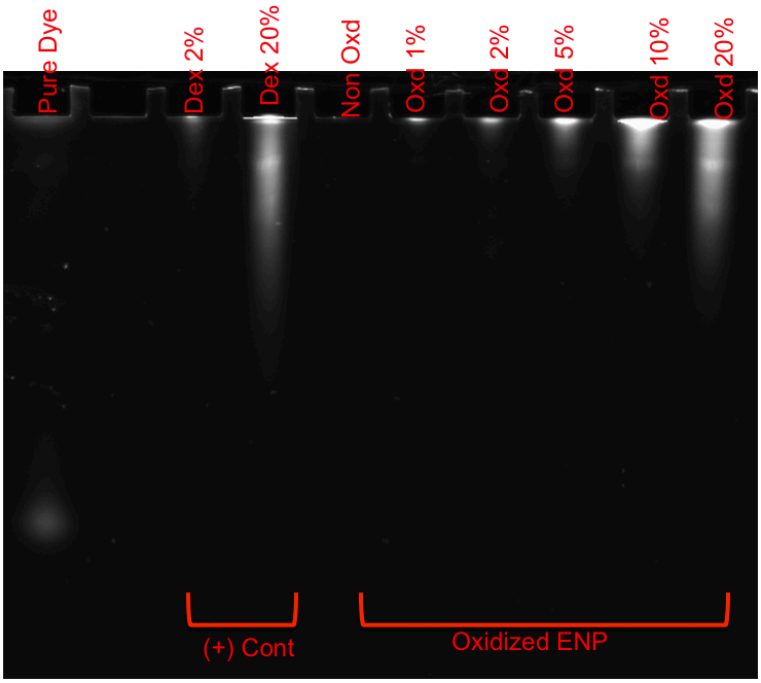

Fig. 19 – Denaturing PAGE results for dye coupled ENPs. First lane, HiLyte Fluor dye used as negative control. The next two lanes, 2% and 20% oxidized dextrin used as positive control. The remaining lanes show ENP samples of various oxidation levels.

The coupling results between dye molecules and ENPs shows promising outcomes. Every oxidation sample displays some level of conjugation and the highest conjugation level is observed in the higher oxidation samples. The next stage of the coupling process is to conjugate control DNA onto the oxidized ENPs. Amine- and Cy3-modified control DNA

Cy3-T15-NH_2 was conjugated with the oxidized samples. Cy3 is a fluorescent dye with emission wavelength of 570 nm; its high stability and extinction coefficient is superior over conventional dyes.

The conjugated products were again diluted and denatured with urea before loading into a gel. Despite the successful attempt for dye molecule coupling, control DNA conjugation was not as optimal. Conjugation result for control DNA was expected to show similar trend to dye coupling result, with the more oxidized samples display higher intensity. However, of all the samples tested, only the 20% oxidized ENP sample shows minimal fluorescent intensity near the top of the well (Fig. 20). None of the other oxidized samples show any conjugation. Residual bands can be seen migrating down the gel, indicating that majority of DNA was wasted and not conjugated. The low conjugation efficiency may be attributed to steric hindrance or electrostatic repulsion. The control DNA is much larger than the dye molecules used in previous conjugation, thus steric effect may have hindered the coupling process. Also, DNA contains negatively charged phosphate groups. Conjugating DNA with carboxyl-bearing oxidized ENPs may be more difficult. To compensate for the low coupling efficiency, reaction parameters must be optimized to reduce DNA waste before conjugation with the aptamer.

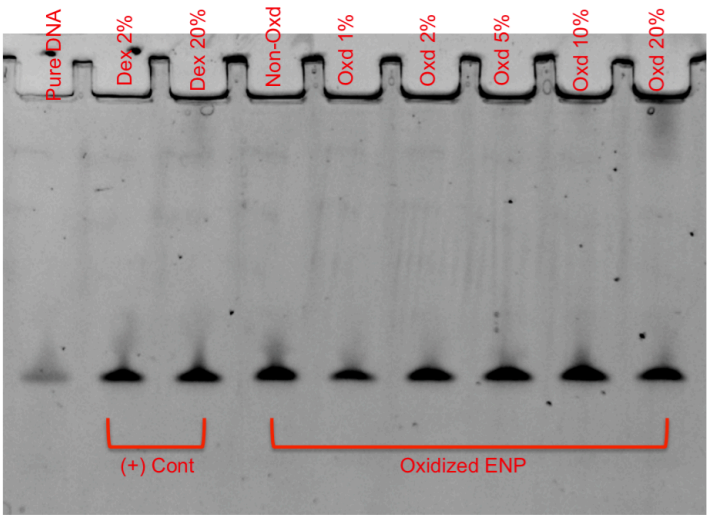

Fig. 20 – Denaturing PAGE results for control DNA-coupled ENPs. First lane, Cy3-T15-NH_2 used as negative control. The next two lanes, 2% and 20% oxidized dextrin used as positive control. The remaining lanes show ENP samples of various oxidation levels.

3.1.2 Optimization of Conjugation Efficiency

To improve the low coupling efficiency, various reaction parameters were tested. Since the previous result shows minor coupling for only the 20% oxidized ENPs, the optimization process were carried out using the 20% oxidized ENPs and the control DNA. The first two parameters investigated were reaction time and pH. Original conjugation were done in pH 7.6 HEPES buffer and reacted for two hours. Some literatures suggest higher yield can be obtained in acidic condition up to pH 4.5. [92], but since EDC hydrolysis is more potent at a low pH, the reaction pHs tested are only slightly acidic. As shown from the optimization result, two sets of reaction time and three different pHs were tested (Fig. 21a). It is clear that a longer reaction time favours conjugation as all three samples that reacted overnight have stronger intensity over their counter parts. As for the different pH, the improvement is less significant, and the lower pH sample shows slightly better performance.

a) b)

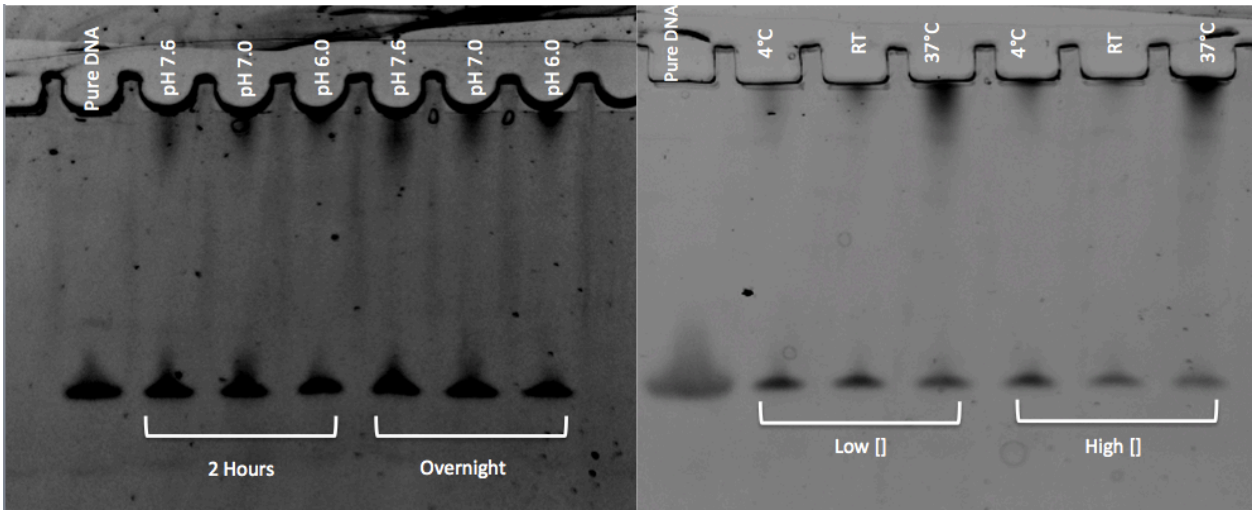

Fig. 21 – Conjugation optimization results a) reaction time and pH b) temperature and DNA:ENPs ratio. A high yield coupling is indicated by a more intense band trapped in the well at the top of the gel.

Following the previously optimized pH and reaction time, the second part of optimization focus on reaction temperature and reagent ratio. Conjugation was carried out at either room temperature, refrigerated 4 °C or slightly heated 35 °C. Two sets of DNA to ENPs ratios were also tested. As shown in Fig. 23, conjugation in heated conditions show dramatic efficiency improvement. This might be attributed to the unfolding of DNA internal structure and thus exposing the amino group for conjugation. A higher DNA to ENP ratio also favours the coupling process. It is worth noting that the right most lane now shows stronger fluorescence from the top coupled band than the bottom residual DNA band. With this encouraging result, the conjugation of aptamer with ENPs was finally carried out using the optimized reaction time, temperature, pH and reagent ratio. The aptamer was also

modified with fluorophore for better observation, and the coupling efficiency was quantified accordingly using the fluorescence intensity of the coupled band and the residual band. Aptamer-coupled ENPs and a diluted sample was measured and the coupling efficiency was found to be over 80% (Fig. 22).

a)

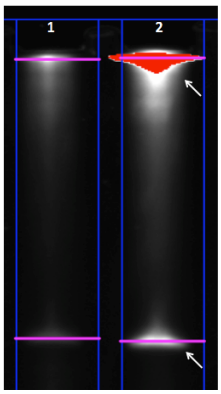

b)

Lane	Coupling Efficiency %
1	81.85%
2	84.64%

Fig. 22 – Aptamers and ENPs conjugation result a) denaturing PAGE results of aptamer coupled ENPs at two different concentration b) coupling efficiency quantification.

3.2 ENPs Precipitation

Throughout the EDC/NHS conjugation process, a very important technique was repeated multiple times to recover ENPs from the aqueous solutions. Ethanol precipitation is a common practice for precipitating and purifying nucleic acids and polysaccharides. [93,94] Ethanol is much less polar than water; when excessive amount of ethanol are added into an aqueous solution, it disrupts the charge screening effect from water. Without charge screening, the dielectric groups on polysaccharides can more easily form ionic bond with ions in the solution and precipitate. During the conjugation process, ENPs were first

reacted with EDC and NHS to activate the carboxyl groups. Activated ENPs were subjected to ethanol precipitation to remove the unreacted reagents then re-dispersed back in water. After the conjugation process, modified ENPs were subject to at least two more ethanol precipitations for purification purpose. It is obvious that ethanol precipitation plays an important role in ENP modification scheme, and therefore it is vital to maximize ENP recovery in every precipitation.

During the aptamer conjugation study, a few observations suggested the possibility of DNA affecting ENP precipitation. A simple experiment was carried out to test this hypothesis. Dye-modified ENPs were synthesized and separated equally into three vials. For the first vial, nothing extra was added into the sample. For the second and the third vial, equal amounts of DNA were added. DNA for vial two was not modified, whereas DNA for vial three has fluorescent labels. All three samples were subject to ethanol precipitation three times before the precipitates were re-dispersed in water and observed with denaturing PAGE (Fig. 23). Sample one precipitated without DNA displayed strikingly low recovery compared to sample two and three. Sample three also shows that DNA facilitates ENP precipitation, and DNA is not associated with ENPs. The free DNA can be clearly seen at the bottom of the gel as a red band since it is labeled with a different fluorophore. The interaction between DN and oxidized ENP is possibly through ionic interaction in ethanol mediated by salt. Once dispersed in water, they can be easily separated.

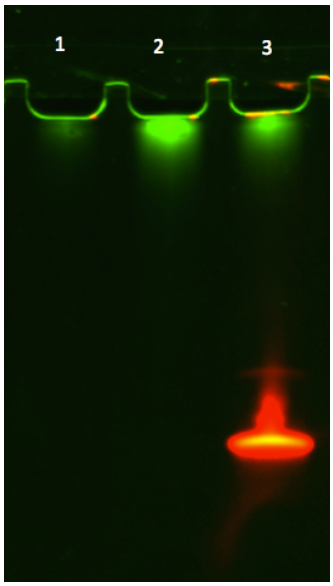

Fig. 23 – ENPs precipitation test 1) 5% (w/w) dye-modified ENPs precipitated using ethanol. 2) 5% (w/w) dye-modified ENPs + non-labeled DNA precipitated with ethanol. 3) 5% (w/w) dye-modified ENPs + fluorophore-labeled DNA precipitated with ethanol.

With this result, further testing was done to quantify the recovery efficiency and to explore better precipitation methods. Dye-modified ENPs were used again with different solvents and additives for precipitation. Precipitates were measured with a fluorometer and calibrated with an external standard to calculate the recovery efficiency. The result suggests that pure ethanol precipitation has a low recovery of less than 40%, and even lower with methanol (Fig. 24). However, precipitation with isopropanol significantly improved the efficiency up to 90%. Samples with additives were also precipitated with ethanol. As expected, the addition of DNA greatly improved ethanol recovery. However, the addition of PEG and salt shows much less improvement.

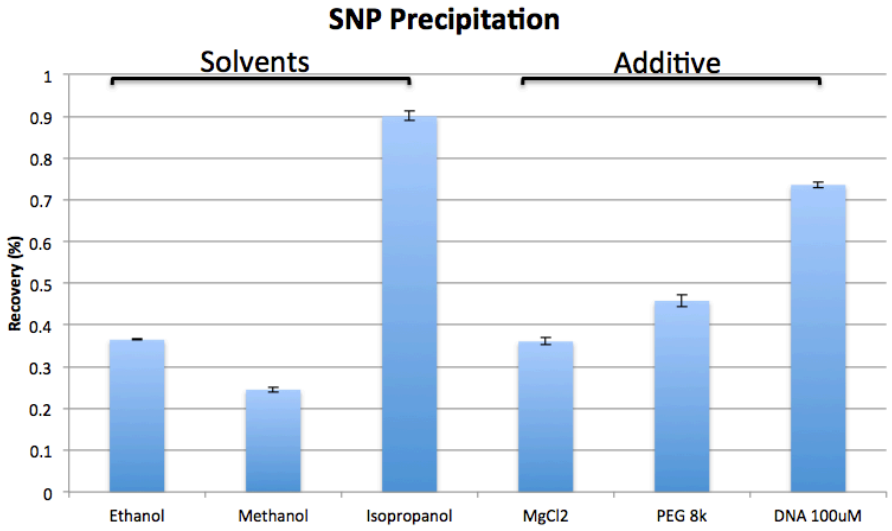

Fig. 24 – ENPs precipitation recovery assay. 5% (w/w) dye-modified ENPs precipitated with different solvents. Dye-modified ENPs mixed with different additive, then precipitated with ethanol.

With the highest recovery rate, isopropanol temporarily replaced ethanol for precipitation and its precipitation capability consistently out-performed the other method. However, it was later discovered that isopropanol precipitation has a detrimental effect on the subsequent internalization study. Therefore, the final precipitation protocol was adjusted back to ethanol precipitation with the addition of salt. Although not as potent as isopropanol, the addition of salt can greatly improve ethanol's recovery (Fig. 25).

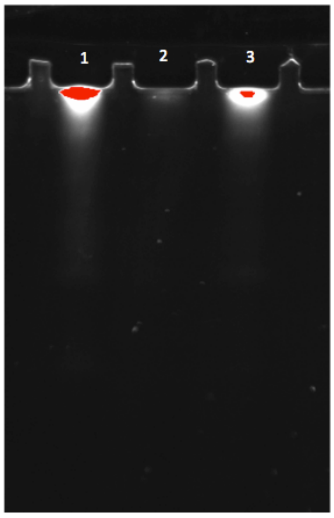

Fig. 25 – 5% (w/w) dye-modified ENP precipitated with 1) 100% isopropanol, 2) 100% ethanol, 3) 100% ethanol + 10 µL of 50 mM $MgCl_2$ salt.

3.3 Materials and Methods

3.3.1 Materials

Isopropanol, ethanol, EDC, and NHS were purchased from Sigma-Aldrich (St. Louis, MO). HEPES and MES buffer were purchased from Amresco (Solon, OH). PEG 8K was purchased from Alfa Aesar (Ward Hill, MA). Control DNA was purchased from Integrated DNA technologies (Coralville, IA). Aptamer AS1411 was purchased from Eurofins (Huntsville, AL). Amine modified dye molecule HiLyte Fluor 488 was purchased from AnaSpec (Fremont, CA). All chemicals were used without any further purification. All aqueous solutions were prepared using Milli-Q water (18.2 MΩ resistivity).

3.3.2 EDC/NHS Aptamer Conjugation

The following protocol describes the optimized reaction condition for the EDC/NHS conjugation. The oxidized ENPs were dispersed in Milli-Q water at 5% (w/w). 40 µL of ENP

solution, 40 μL of 0.5 M pH 6.0 MES buffer, 40 μL of 0.5 M EDC and 40 μL of 0.025 M NHS were mixed consecutively. The reaction vial was placed on a block heater overnight at 35 °C. 10 μL of 10 mM $MgCl_2$ was added into the reaction mixture before precipitation with 1 mL of ethanol. The precipitate was cooled in the fridge for 15 minutes and centrifuged at 15000 rpm for 5 minutes to recover activated ENPs. ENPs were re-dispersed in 40 μL of Milli-Q water and the aptamer/dye solution was added. The reaction was, again, left on block heater for 12 hours then precipitated with ethanol and salt for two more times before re-dispersed in 40 μL of Milli-Q.

3.3.3 Gel Electrophoresis

To prepare for the poly-acrylamide gel, 22 mL of 10% polyacrylamide solution was mixed with 50 μL of 10% ammonium persulfate (APS), and 20 μL of tetramethylethylenediamine (TEMED). The mixture was loaded into a prepared molding cassette and set for 40 minutes. Sample wells were washed three times with buffer. Testing samples were mixed with equal amounts of 8 M urea before loading into sample wells. Denaturing PAGE was ran at 500 V, 250 mA and 30 W for 40 minutes.

Chapter 4. Cellular Uptake of ENPs

The last chapter of this thesis is to test our vehicle's capability in terms of selective cellular internalization. The ENPs have been modified with aptamers for active targeting. Therefore, the first task is to investigate whether or not cancer cells can selectively internalize the aptamer-modified vehicle. To visualize internalization, the ENPs are either directly modified with dye molecules or the attached aptamers have fluorescent labels. Internalization studies were observed and imaged using fluorescence microscopy. The internalization results are compared against liposome-based vehicles.

4.1 Cellular Internalization

The aptamer used for the previous conjugation is AS1411. AS1411 is a 26-base guanine-rich DNA aptamer with the sequence 5'-GGTGGTGGTGGTTGTGGTGGTGGTGG. Among all the therapeutic aptamers, AS1411 is one of the most advanced aptamer for cancer treatment. [95] *In-vivo* studies for AS1411's antitumor activity suggest delayed tumor growth for renal cancer, lung cancer, and breast cancer xenograft. Phase I clinical trials also show promising result of stabilizing cancer growth. [96]

Aside from the growth inhibition capability, AS1411 also shows strong affinity to specific cancer cells [97] like the MCF-7 breast cancer, MV4-11 Leukemia, and HeLa cervical cancer cells. Research has attributed this phenomenon to AS1411's affinity toward the nucleolin protein on the plasma membrane. AS1411 oligonucleotides usually dimerize to form a higher structure consisting of eight G-quartets. The G-quartets' structure greatly improves the aptamers' stability and is essential for AS1411's affinity towards nucleolin. [98] Nucleolin is generally a nucleolar protein but can sometimes be found on the cell

membrane surface. The membrane nucleolin has relatively low expression on normal cells but is overexpressed on many different types of cancer cells. The membrane nucleolin works in conjunction with actin filaments and acts as a shuttling protein between the cytoplasm and the nucleus. [99] The detailed mechanism of action for AS1411 is still not clear, but studies have shown that once AS1411 binds with a membrane nucleolin, it triggers internalization. The aptamer and nucleolin complex further interact with other cofactors and eventually inhibits DNA replication (Fig. 26).

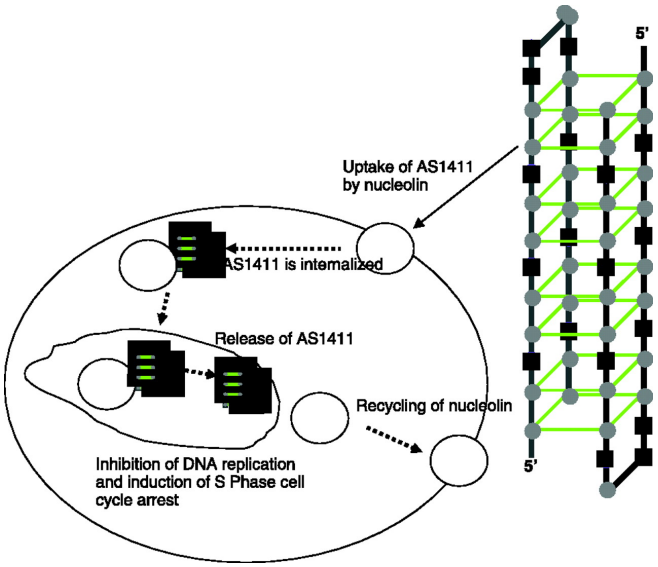

Fig. 26 – Proposed AS1411 mechanism of action. AS1411 oligonucleotides dimerize to form eight G-quartets and interact with membrane nucleolin to trigger internalization. This figure is adapted from ref. [98]. Copyright 2006, American Association for Cancer Research.

4.2 Microscopic Imaging

4.2.1 Epifluorescence Microscopy

The internalization results were first observed using epifluorescence microscopy. For sample preparation, aptamer- and control DNA-modified ENP samples were incubated with

HeLa cells in 96-well plate. 50 nm fluorescein isothiocyanate (FITC)-labeled silicon beads were also incubated with HeLa cells and used as positive control. For better visualization, cell nuclei were stained with the Hoechst 33258 dye. The illustrations on the left represent the samples incubated with cells. The dashed circle represents an ENP, the filled circle represents a silicon bead, the folded line represents the aptamer AS1411, the unfolded line represents control DNA and star represents fluorophore (Fig. 27). The blue channel shows the stained cell nuclei, the green channel shows the signal from ENPs or silicon beads and the merged channel displays a stacking image of all three channels to show localization. A number of problems were discovered from this initial result. Firstly, the cell nuclei show no obvious signal even under strong exposure. Secondly, ENP samples display no internalization. The signal observed from the positive control is much stronger but contains a lot of background fluorescence in areas where cells are not present. These defects are possibly caused by live observation as live cells have lower staining efficiency. Therefore, to better evaluate modified ENPs' internalization, a different staining and imaging technique is required.

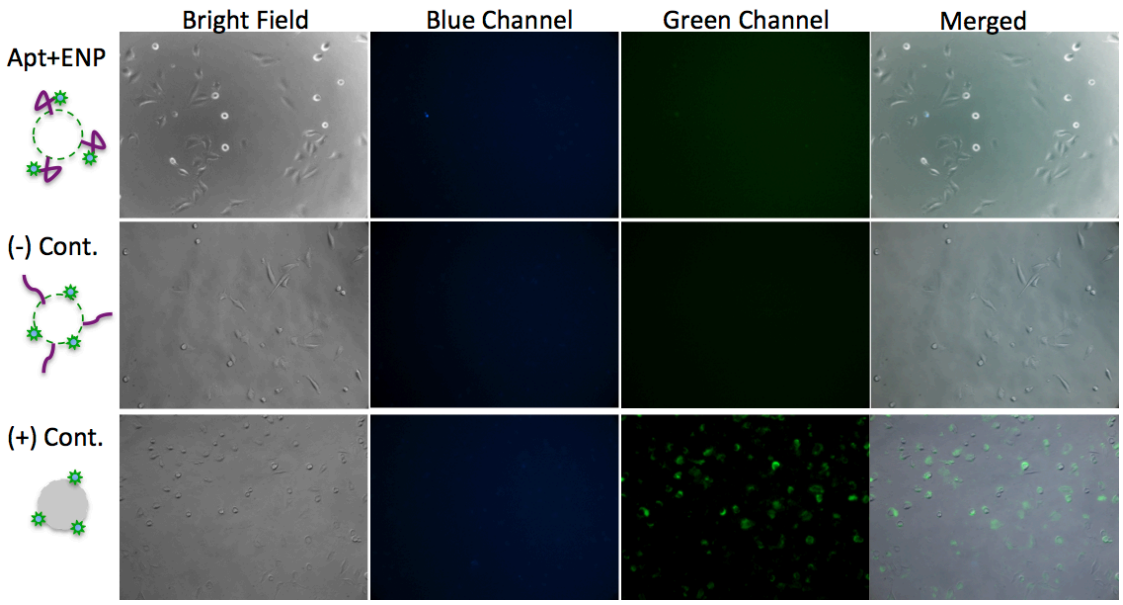

Fig. 27 – Epifluorescence microscopy images of cellular internalization assay. From top to bottom, aptamer-modified ENPs, random DNA-modified ENPs as negative control, and dye-modified 50 nm silicon beads as positive control.

4.2.2 Confocal Laser Scanning Microscopy

Confocal microscopy is an advanced technique of fluorescence microscopy with a significant improvement on optical resolution and contrast. This improvement comes from the addition of optical pinholes at both the light source and the detector to eliminate out of focus light. The cellular samples subject to confocal microscopy were also fixed with paraformaldehyde and stained with 4',6-diamidino-2-phenylindole (DAPI). The same samples from previous epifluorescence microscopy attempts were incubated with HeLa cells on circular coverslips in a 24-well plate. Compared with the previous result, confocal images have much higher resolution and stronger contrast (Fig. 28). Cell nuclei are also clearly visible with DAPI stain. It is important to note that the images were acquired under different imaging parameters to showcase the contrast between confocal microscopy and

epifluorescence microscopy. No quantitative comparison can be made between the three tested samples.

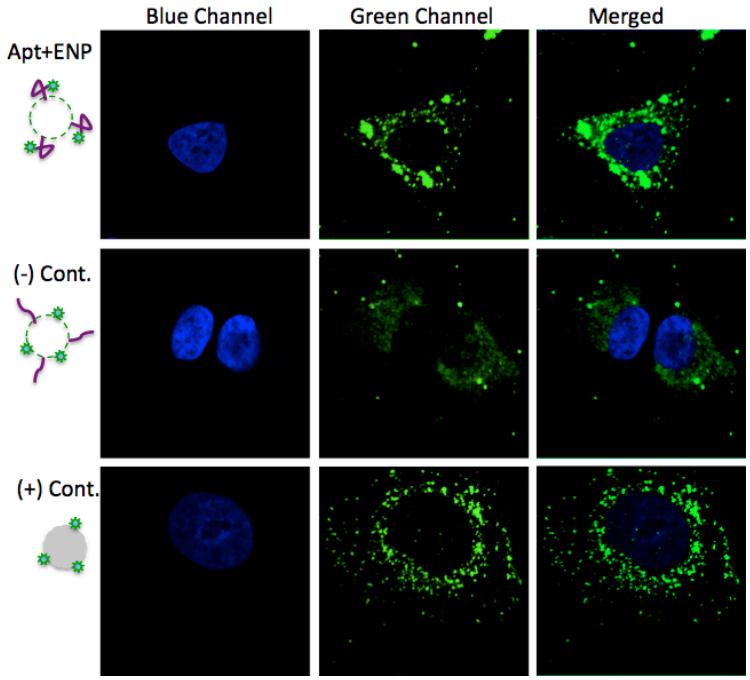

Fig. 28 – Confocal microscopy images of cellular internalization assay. From top to bottom, aptamer-modified ENPs, random DNA-modified ENPs as negative control, and dye-modified 50 nm silicon beads as positive control. Blue channel shows stained nuclei, green channel shows fluorescent from aptamers, ENPs or silicon beads.

4.3 Vehicle Internalization Assay

With the proper imaging technique to visualize cellular internalization, different samples of modified ENPs were synthesized to evaluate the vehicle's capability.

4.3.1 Aptamer Density

The first internalization study is to investigate the effect of aptamer density on ENPs. Three samples of modified ENPs were prepared, one with no aptamers but dye molecules

and the two other samples have different ENP:aptamer molar ratio at 1:1 and 1:0.2. The ENP:DNA ratios were calculated based on the assumption of ENP molar weight of 10^6 Dalton. All the imaging parameters were kept consistent for unbiased comparison. As shown in confocal images, both samples of aptamer-modified ENPs display clear internalization. Interestingly, dye-modified ENPs also show strong internalization comparable to the high aptamer ratio sample. It needs to be pointed out here that the fluorophore label is starch for this sample, while the two DNA containing samples have their label on DNA. Therefore, the fluorescence intensity of these samples is not directly comparable. This result suggests ENPs can be internalized by HeLa cells without the help of aptamers. As for aptamer modification, the effect of aptamer density is not conclusive.

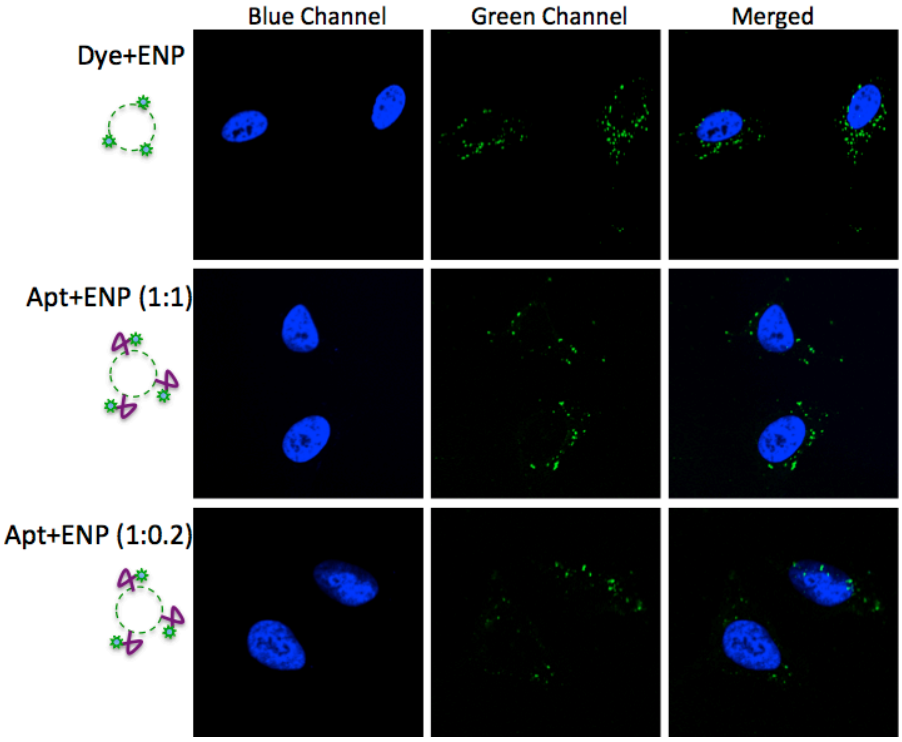

Fig. 29 – Internalization assay, aptamer density study. From top to bottom, dye-modified ENPs, high aptamer-ratio aptamer-modified ENPs, low aptamer-ratio aptamer-modified ENPs.

4.3.2 Dual-Labeled Vehicle Assay

To further validate ENPs' internalization and aptamers' density effect, dual-labeled modified ENPs were prepared. ENPs were first conjugated with Cy5 labeled AS1411 then with HiLyte Fluor 488 dye. The dual-labeled ENPs can be observed under a different wavelength to probe co-localization. HeLa cells' actin filaments were also stained to better visualize ENPs' intracellular location. The green channel shows ENPs' location, the red channel shows aptamer fluorescence and the yellow channel shows the approximate location of the cell membrane. As shown in the confocal images, the dual-labeled ENPs' internalization result is in good agreement with the previous attempt. The dye modified ENP sample displays clear internalization (Fig. 30). Both of the aptamer-modified samples were internalized. Most of the signals observed in red channel are co-localized with ENPs' fluorescence. This overlap further confirms that the signal observed is from aptamer-modified ENPs and not from non-specific fluorescence.

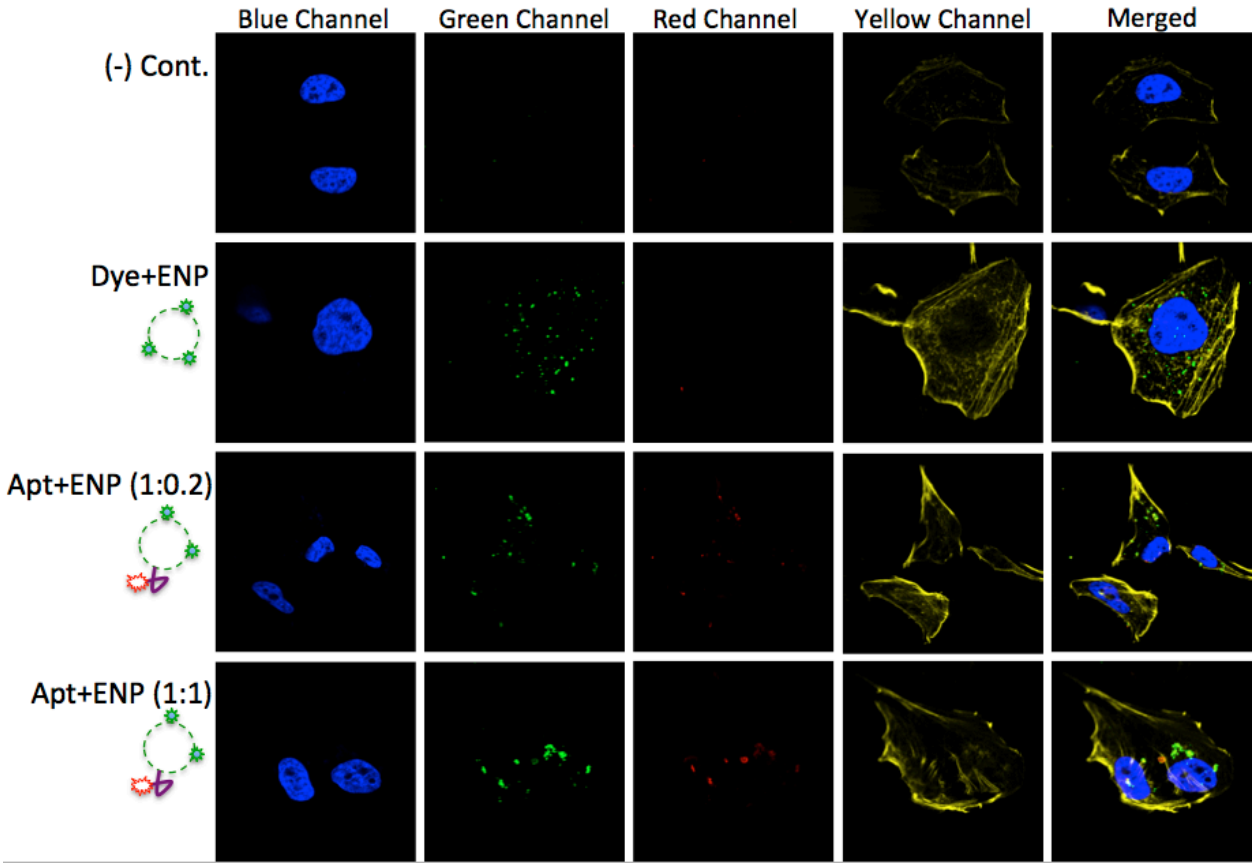

Fig. 30 – Internalization assay, duo labeled ENPs. From top to bottom, the negative control contained no samples, dye-modified ENPs, low aptamer-ratio aptamer-modified ENPs, high aptamer-ratio aptamer-modified ENPs.

4.4 Vehicle Selectivity Assay

The second part of the modified ENPs' evaluation investigates the vehicle's specificity. As mentioned previously, one of the major problems for chemotherapy is unintentional cytotoxicity. It is highly desirable for a drug delivery vehicle with the capability to distinguish its target. AS1411's affinity toward nucleolin facilitates ENP targeting and HeLa cell internalization. Theoretically, conjugating another aptamer with a different molecular target would significantly reduce the vehicle's selective internalization. Sgc8 is a DNA

aptamer selected using cell-SELEX with strong affinity towards acute lymphoblastic leukemia. [100] Studies have shown sgc8's molecular target is also a membrane protein but instead of nucleolin, sgc8 binds to tyrosine kinase. [101] Four samples of aptamer-modified ENPs were made to test vehicle's selectivity. Two samples with AS1411 at different ENP:DNA ratio and the other two with sgc8. AS1411-conjugated samples behaved as expected, internalization was observed and aptamer fluorescence co-localized with the ENP signal (Fig. 31). On the contrary, sgc8-modified samples showed no obvious internalization. The aptamer signal shows no response and the slight green fluorescence might be caused by the non-conjugated ENPs. This result demonstrated the highly selective nature of aptamer conjugated ENPs.

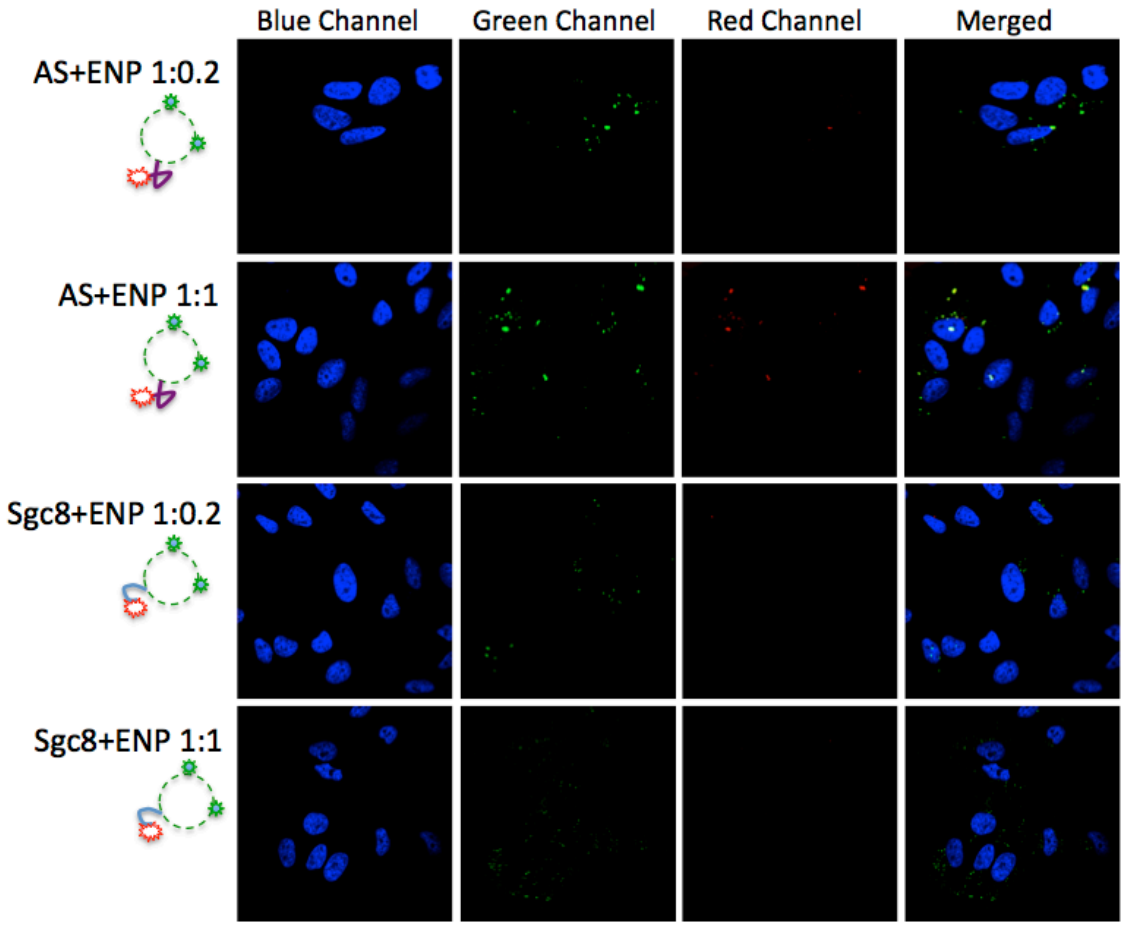

Fig. 31 – Vehicle selectivity assay. The first two samples are AS1411-modified ENPs (HeLa targeting) at two different aptamers:ENPs ratios. The bottom two samples are sgc8-modified ENPs (non-HeLa targeting) at the same two ratios.

4.5 Internalization Efficacy Comparison – Liposome

The previous assays reveal the modified ENPs' capability in terms of internalization and selectivity. For the purpose of comprehensive study, modified ENPs are subject to benchmarking against the market standard liposome. The liposomes tested composed of 94% 1,2-Dioleoyl-sn-glycero-3-phosphocholine (DOPC), 5% MPB-PE and 1% Rhodamine-

labeled DOPC. Liposomes were extruded through 100 nm membrane, which yielded mean size of around 114 nm. The addition of MPB-PE provides conjugation site for thiolated DNA.

Rhodamine-labeled liposomes were conjugated with thiol-modified AS1411 before being subjected to the internalization test. As shown in the test result, both aptamer-modified ENPs and liposome show significant cellular uptake. Nonetheless, uptake extent in the liposome sample is much higher than the ENP sample. Another important detail is that the ENP sample concentration is orders of magnitude higher than the liposome sample. The difference in concentration further amplifies the contrast in internalization efficacy. The non-modified liposome shows no internalization.

It is interesting that the initial result suggests similar uptake behaviour for both the modified, and non-modified liposome (Fig. 32). Cellular internalization of non-modified liposome is caused by the binding of serum protein to the non-conjugated MPB-PE sites. Thiol group of cysteine residues on serum protein can forms covalent bond with the maleimide group on MPB-PE. The protein-coated liposome is favourable for cellular internalization. Capping the conjugation site with mercaptoethanol compensated this artefact.

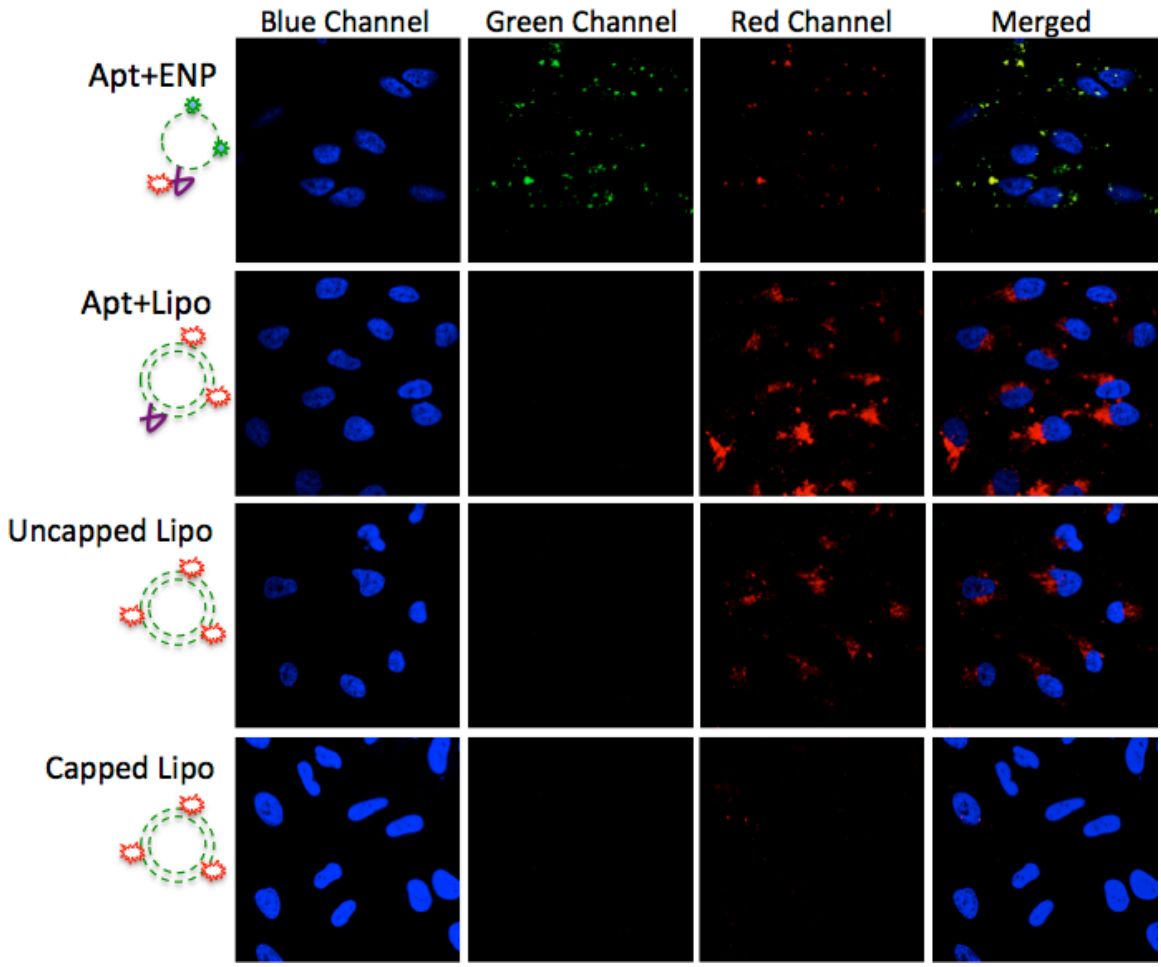

Fig. 32 – Internalization comparison, aptamer modified ENPs, aptamer modified liposomes and dye-labeled liposomes.

4.6 Materials and Methods

4.6.1 Materials

Fluoromount, BSA and Triton X-100 were purchased from Sigma Aldrich (St. Louis, MO). Mercaptoethanol was purchased from Alfa Aesar (Ward Hill, MA). Paraformaldehyde and Alexa Fluor 448 Phalloidin dye were purchased from Fisher Scientific (Waltham, MA). Dulbecco's Modified Eagle Medium (DMEM) and Dulbecco's Phosphate Buffered Saline (DPBS) were purchased from Lonza (Allendale, NJ). DOPC, Rhodamine labeled DOPC, and

MPB-PE were purchased from Avanti (Alabaster, AL). Dithiothreitol was purchased from Amresco (Solon, OH). Cy5 labeled AS1411 and thiolated AS1411 were purchased from Eurofin (Huntsville, AL). Sep Pak column was purchased from Waters (Mississauga, ON). All chemicals were used without any further purification. All aqueous solutions were prepared using Milli-Q water (18.2 MΩ resistivity). HeLa cell line (CCL-™) was obtained from the American Type Culture Collection (ATCC Manassas, Virginia) through the help of Dr. Shirley Tang (Waterloo, ON).

4.6.2 Cell Culture

HeLa cells were cultured with DMEM/F12 medium containing 10% (v/v) fetal bovine serum, 10% (v/v) of 100 U/mL penicillin-streptomycin and incubated in humidified 5% CO_2 incubator at 37 °C. Cells were seeded onto 14 mm coverslips in a 24-well plate at density of 20,000 cells per well. 500 µL of culture medium were added into the well and incubated overnight before adding 10 µL of samples. Cellular samples were incubated overnight before fixing and staining.

4.6.3 Confocal Laser Scanning Microscopy

The following protocol describes the sample preparation and staining procedures for confocal laser scanning microscopy. Sample-containing medium were removed and the coverslips were washed twice with 500 µL of DPBS. Cells were fixed 200 µL of 4% paraformaldehyde for 10 minutes at room temperature. Cells were washed twice with 500 µL DPBS after fixing. 200 µL of 0.1% Triton X-100 was added to cells for 3 to 5 minutes, then washed two more times with 500 µL DPBS. Fixed cells were incubated with 200 µL

DPBS containing 1% BSA for 20 minutes to prevent non-specific staining. Cells were again washed twice with DPBS then stained with Alexa Fluor 448 Phalloidin dye at 1 unit concentration per sample for 20 minutes at room temperature. Samples were washed twice again with DPBS before the final staining with 200 µL of 2% DAPI for 5 minutes. The final samples were washed and submerged in DPBS. 30 µL for Fluoromount was added onto cleaned microscope slide, and the sample coverslip was placed cell side down onto the Fluoromount droplet. Slides were left to dry overnight before ready to be observed under the microscope. Samples were observed and imaged using a Zeiss LSM 510 Meta Confocal Microscope.

4.6.4 Liposome Preparation

Thiol-modified AS1411 was activated with dithiothreitol for one hour at room temperature. The activated DNA was passed through a Sep Pak column to de-salt and was quantified using a NanoDrop UV-Vis Spectrophotometer. Prepared 114 nm DOPC liposomes containing 5% MPB-PE and 1% Rhodamine-labeled DOPC were diluted to 10nM using HEPES. 1 µL of activated AS1411 were conjugated with 50 µL of 10 nM liposomes in 100 µL of 10 mM pH 7.4 HEPES overnight. The DNA-modified liposomes were precipitated using centrifugation (130000 rpm) at 4 °C, the supernatant was removed and the precipitates were re-dispersed in 10 mM HEPES.

Chapter 5. Conclusion and Recommendations

5.1 Conclusion

This thesis began with an examination of global cancer pandemic and cancer history. The examination is followed by a comprehensive review of the three major cancer treatments, surgical operation, radiation therapy and chemotherapy. Chemotherapeutics were reviewed in detail and one of the solutions for its non-specific cytotoxicity is to incorporate drugs within targeted delivery vehicles. Targeted drug delivery was then investigated in detail in terms of targeting methods, vehicle compositions, and biocompatibility. Seeing that biodegradable nanoparticles have attracted much attention in the field of drug delivery, the focus then shifted onto polysaccharides-based systems and more specifically starch nanoparticles. After an in-depth review of starch's fundamental characteristics and its applications, we recognized that a commercially available starch nanoparticle named EcoSphere™ serves as an excellent platform for anticancer-targeted drug delivery. Two major modifications were proposed to improve ENPs' targeting capability, namely oxidation and aptamer conjugation. The final study focused on evaluating the modified vehicle's capabilities such as cellular internalization and selectivity.

The first modification equipped ENPs with conjugation sites for subsequent aptamer coupling. Specifically, C6 hydroxyls on glucose units were partially oxidized to carboxyl groups using TEMPO catalyst. 1%, 2%, 5%, 10%, and 20% partially oxidized ENP samples were prepared. Spectroscopic measurements were used to confirm oxidation and characterize oxidized ENPs' properties. ^{1}H NMR confirmed oxidation with 9.1ppm aldehyde shift showing signal strength proportional to oxidation level. ^{13}C NMR displayed two carbonyl shifts representing the two oxidized product, aldehyde and carboxyl. All of the

oxidized samples subject to FTIR showed significant carbonyl peak at around 1600 cm^{-1}. DLS size measurements suggested possible ENP aggregation for the higher oxidized samples. And finally, ζ-potential measurements showed decreasing trend along with increasing carboxyl groups for the oxidized samples.

The second modification utilized ENP's newly introduced carboxyl groups for aptamers conjugation. Zero-length linkage between ENP carboxyl and amine-modified aptamers were accomplished through EDC/NHS conjugation. Every sample from the previous modification was first conjugated with dye molecules and control DNA to investigate the optimal oxidation level for conjugation. Conjugated products were analyzed using denaturing PAGE and the initial result only showed successful coupling with the dye molecules. Minor DNA conjugation was observed for only the 20% oxidized ENPs. To improve DNA conjugation efficiency, reaction parameters were optimized for time, temperature, pH and reagent ratios. Using the optimized reaction conditions, aptamers were coupled with 20% oxidized ENPs and the coupling efficiency was greatly improved to above 80%. Aside from conjugation optimization, the ENP precipitation procedure was also enhanced. The original precipitation method with ethanol showed significant ENP loss. A number of different solvents and additives were tested to enhanced ENP recovery. The final precipitation method was modified to co-precipitation conjugated ENPs with $MgCl_2$ salt.

With the ENPs fully modified, the final study focused on evaluating the vehicle's capability. Vehicle cellular internalization and vehicle selectivity were investigated and observed using fluorescence microscopy. Initial epifluorescence microscopy results were crude and produced no conclusive evidence. A different imaging and staining technique

were tested and the resulting images showed significant improvement. Initial internalization assay confirmed cellular internalization for aptamer-modified ENPs, and the dye-modified ENPs also displayed significant internalization. Dual-labeled vehicle assay further confirmed internalization with co-localized ENPs and aptamer fluorescence. Vehicle selectivity was validated through HeLa cells' preferential uptake of AS1411-modified ENPs over sgc8-modified ENPs. Lastly, aptamer-modified ENPs were subjected to benchmarking against aptamer-modified liposomes. Benchmarking results showed significantly higher uptake efficiency for liposomes over ENPs.

5.2 Recommendations

The results described in this thesis show great potential for aptamer-modified ENPs as a targeted anti-cancer drug delivery vehicle. However, further studies are needed to fully understand and improve the vehicle's performance. The author recommends the following four aspects for future works: 1) modified vehicle characterization, 2) drug loading efficiency and release profile, 3) quantitative analysis for cellular internalization using flow cytometry, 4) selectivity test using different cell lines and the corresponding aptamers and 5) perform vehicle modification using larger ENP.

1) Modified vehicle characterization

Vehicle characterization such as size and ζ-potential measurements was only done with the oxidized ENP samples. Similar measurements for the aptamer-modified ENPs are essential to better comprehend their fundamental property. Vehicle toxicity should also be investigated. Toxicity studies on non-modified ENPs suggest no obvious cytotoxicity.

However, after numerous modifications, it is possible for the resulting vehicle to have a negative effect on cell proliferation.

2) Drug loading efficiency and release profile

As a drug delivery platform, one of the major objectives is the ability to incorporate therapeutic molecules and achieve sustained release. It is a common practice for a drug delivery study to investigate the vehicle's encapsulation efficiency and establish its release profile. A popular model drug for such study is doxorubicin due to its fluorescence.

3) Quantitative analysis for cellular internalization

All of the internalization assays presented in this thesis produced only qualitative evidence. Quantitative analysis was attempted by measuring the fluorescence intensity in the medium after internalization test, but the results were inconclusive. Flow cytometry utilized single cell counting technique to more accurately quantify cellular internalization.

4) Selectivity test using different cell lines and the corresponding aptamers

All of the internalization assays and selectivity assay presented in this thesis were done using HeLa cells. To further emphasize the vehicle's selectivity, separate ENP samples modified with different aptamers and dyes can be incubated with cell samples containing different cell lines.

5) Vehicle modification using larger ENP

The molecular weight of ENP is around 10^6 Dalton from our collaborators. The molecular weight of AS1411 is around 12000 Dalton. Therefore, if one ENP is conjugated to just one aptamer, the weight of aptamer needed is 1.2% of the ENP. If we consider the coupling efficiency and if more than one DNA is attached to each ENP, the mass ratio between aptamer and ENP is likely to go over 1:100. While ENP is cost-effective, the aptamer is more costly. Therefore, it might be necessary to engineer higher molecular weight ENP to decrease the usage of aptamer.

References

1. Cooper, G.M. Elements of Human Cancer; Jones and Bartlett Publishers: Boston, 1992.
2. Stewart, B.W.; Wild, C.P. World Cancer Report 2014. International Agency for Research on Cancer: Lyon, 2014
3. Boyle, P.; Levin, B. World Cancer Report 2008. International Agency for Research on Cancer: Lyon, 2008.
4. Cancer Facts & Figures 2012. American Cancer Society: Atlanta, 2012.
5. Jemal, A.; Bray, F.; Center, M.M.; Ferlay, J.; Ward, E.; Forman, D. Global Cancer Statistics. CA A Cancer Journal for Clinicians. **2011**, 21, 69-90.
6. Miller, A.B.; Hoogstraten, B.; Staquet, M.; Winkler, A. Reporting results of cancer treatment. Cancer. **1981**, 47, 207-214.
7. Hajdu, S.I. A note from history: landmarks in history of cancer, part 4. Cancer. **2012**,118,4914-4928.
8. Wood, W. X-rays in the treatment of cancer and other malignant diseases. The Medical Record. **1902**, 62, 692-695.
9. Rak, J.; Chomicz, L.; Wiczk, J.; Westphal, K.; Zdrowowicz, M.; Wityk, P.; Zyndul, M.; Makurat, S.; Golon, L. Mechanisms of damage to DNA labeled with electrophilic nucleobases induced by ionizing or UV radiation. The Journal of Physical Chemistry. **2015**, 119, 8227-8238.
10. Kerr, J.F.R.; Winterford, CM.; Harmon, B.V. Apoptosis – Its significance in cancer and cancer therapy. Cancer. **1994**, 73, 2013-2026.

11. Karnofsky, D.A.; Walter, H.A.; Lloyd, F.C.; Joseph, H.B. The use of the nitrogen mustards in the palliative treatment of carcinoma. With particular reference to bronchogenic carcinoma. Cancer. **1948**, 1, 634-656.
12. Hegi, M.E.; Diserens, A.; Gorlia, T.; Hamou, M.; de Tribolet, N.; Weller, M.; Kros, J.M.; Hainfellner, J.A.; Mason, W.; Mariani, L.; Bromberg, J.E.C.; Hau, P.; Mirimanoff, R.O.; Cairncross, J.G.; Janzer, R.C.; Stupp, R. MGMT gene silencing and benefit from temozolomide in glioblastom. New England Journal of Medicine. **2005**, 352, 997-1003.
13. Kaufmann, S.H.; Earnshaw, W.C. Induction of apoptosis by cancer chemotherapy. Experimental Cell Research. **2000**, 256,4 2-49.
14. Liu, J.F.; DNA topoisomerase poisons as antitumor drugs. Annual Review of Biochemistry. **1989**, 58, 351-375.
15. Gibson, R.J.; Keefe, D.M. Cancer chemotherapy-induced diarrhea and constipation: mechanisms of damage and prevention strategies. Supportive Care in Cancer. **2006**, 24, 890-900.
16. Neog, B.; Sinha, S.; Bhttacharyya, P.K. Alkylation of DNA by nitrogen mustards: A DFT study. Computational and Theoretical Chemistry. **2013**, 1018, 19-25.
17. Jordan, K; Sippel, C.; Schmoll, H.J. Guidelines for antiemetic treatment of chemotherapy-induced nausea and vomiting: past present and future recommendations. Oncologist. **2007**, 12, 1143-1150.
18. Katzel, J.A.; Fanucchi, M.P. Recent advances of novel targeted therapy in non0small cell lung cancer. Journal of Hematology & Oncology. **2009**, 2, 1-18.

19. Ducry, L.; Stump, B. Antibody-drug conjugates: linking cytotoxic payloads to monoclonal antibodies. Bioconjugate Chemistry. **2010**, 21, 5-13.
20. Stephen, C.A.; Nicole, M.O.; Peter, D.S. Antibody-drug conjugates: targeted drug delivery for cancer. Current Opinion in Chemical Biology. **2010**, 14, 529-537.
21. Peters, G.J.; van der Wilt, C.L.; Van Moorsel, C.J.A.; Kroep, J.R.; Bergman, A.M.; Ackland, S.P. Basis for effective combination cancer chemotherapy with antimetabolites. Pharmacology & Therapeutics. **2000**, 87, 227-253.
22. Lam, P.L.; Gambari, R. Advanced progress of microencapsulation technologies: in vivo and in vitro models for studying oral and transdermal drug deliveries. Journal of Controlled Release. **2014**, 178, 25-45.
23. Brannon-Peppas, L.; Blanchette, J.O. Nanoparticle and targeted systems for cancer therapy. Advanced Drug Delivery Reviews. **2004**, 56, 1649-1659.
24. Jong, D.W.; Borm, J.A. Drug Delivery and nanoparticles: Applications and hazards. International Journal of Nanomedicine. **2008**, 2, 133-149.
25. Ferrari, M. Cancer nanotechnology: opportunities and challenges. Nature Review Cancer. **2005**, 5, 161-171.
26. Ishida, T.; Harashima, H.; Kiwada, H. Liposome clearance. Bioscience Reports. **2002**, 22, 197-224.
27. Li, X.; Yu, Y.; Ji, Q.; Qiu, L.Y. Targeted delivery of anticancer drugs by aptamer AS1411 mediated Pluronic F127/cyclodextrin-linked polymer composite micelles. Nanomedicine-Nanotechnology Biology and Medicine. **2015**, 11, 175-184.

28. Gujral, S.; Khatri, S. A review on basic concept of drug targeting and drug carrier system. International Journal of advances in Pharmacy, Biology and Chemistry. **2013**, 2, 130-136.
29. Duncan, R.; Sat, Y. Tumour targeting by enhanced permeability and retention (EPR) effect. Annals of Oncology. **1998**, 39.
30. Greish, K. Enhanced permeability and retention effect for selective targeting of anticancer nanomedicine: Are we there yet? Drug Discovery Today. **2012**, 9, 161-166.
31. Maeda, H.; Wu, J.; Sawa, T.; Matsumura,; Y. Hori, K. Tumor vascular permeability and the EPR effect in macromolecular therapeutics: a review. Journal of Controlled Release. **2000**, 65, 271-284.
32. Lembo, D.; Cavalli, R. Nanoparticulate delivery systems for antiviral drugs. Antiviral Chemistry & Chemotherapy. **2010**, 21, 53-70.
33. Lembo, D.; Cavalli, R. Review – Nanoparticulate delivery systems for antiviral drugs. Antiviral Chemistry & Chemotherapy. **2010**,21,53-70.
34. Torchilin, V.P.; Klibanov, A.L.; Huang, L.; O'Donnell, S.; Nossiff, N.D.; Khaw; B.A. Targeted accumulation of polyethylene glycol-coated immunopiposomes in infracted rabbit myocardium. The Journal of the Federation of American Societies for Experimental Biology. **1992**, 6, 2716-2719.
35. Bies, C.; Lehr, C.; Woodley, F. J. Lectin-mediated drug targeting: history and applications. Advanced Drug Delivery Reviews. **2004**,56,425-435.
36. Torchilin, V.P. Passive and active drug targeting: drug delivery to tumors as an example. Handbook of Experimental Pharmacology. **2010**, 197, 3-53.

37. Xiao, S.; Tong, C.; Liu, X.; Yu, D.; Liu, Q.; Xue, C.; Tang, D.; Zhao, L. Preparation of folate-conjugated starch nanoparticles and its application to tumor-targeted drug delivery vector. Chinese Science Bulletin. **2006**, 51, 1693-1697.
38. Li, Xin.; Zhao, Q.; Qiu, L. Smart ligand: aptamer –mediated targeted delivery of chemotherapeutic drugs and siRNA for cancer therapy. Journal of Controlled Release. **2013**, 171, 152-162.
39. Veli C. Ozlp and Thomas Schafer (2012). Aptamer-Nanoparticle Bioconjugates for Drug Delivery, The Delivery of Nanoparticles, Dr. Abbass A. Hashim (Ed.), ISBN: 978-953-51-0615-9. In Tech.
40. Brannon-Peppas, L.; Blanchette, J.O. Nanoparticle and targeted systems for cancer therapy. Advanced Drug Delivery Reviews. **2012**, 64, 206-212.
41. Lee, J.H.; Yigit, M.V.; Mazumdar, D.; Lu, Y. Molecular diagnostic and drug delivery agents based on aptamer-nanomaterial conjugates. Advanced Drug Delivery Reviews. **2010**,62,592-605.
42. Yang, L.; Zhang, X.; Ye, M.; Jiang, J.; Yang, R.; Fu, T.; Chen, Y.; Wang, K.; Liu, C.; Tan, W. Aptamer-conjugated nanomaterials and their applications. Advanced Drug Delivery Reviews. **2011**, 63, 1361-1370.
43. Lee, J.H.; Yigit, M.V.; Mazumdar, D.; Lu, Y. Molecular diagnostic and drug delivery agents based on aptamer-nanomatierls conjugates. Advanced Drug Delivery Reviews. **2010**, 62, 592-605.
44. Darmostuk, M.; Rimpelova, S.; Gbelcova, H.; RumL, T. Current approaches in SELEX: An update to aptamer selection technology. Biotechnology Advances. **2015**.

45. Zamboni, W.C. Liposomal, nanoparticle, and conjugated formulation of anticancer agents. Clinical Cancer Research. **2005**, 11, 8230-8234.

46. Matsumura, Y.; Maeda, H. A new concept of macromolecular therapies in cancer chemotherapy: mechanism of tumortropic accumulation of proteins and the antitumor agent SMANCS. Cancer Research. **1986**, 6, 6387-6392.

47. Hong, S.; Leroueil, P.R.; Majoros, I.J.; Orr, B.G.; Baker, J.R.Jr.; Banaszak Holl, M.M. The binding avidity of a nanoparticle-based multivalent targeted drug delivery platform. Chemistry & Biology. **2007**, 14, 107-115.

48. Bartlett, D.W.; Davis, M.E. Physiochemical and biological characterization of targeted, nucleic acid-containing nanoparticles. Bioconjugate Chemistry. **2007**, 18, 456-468.

49. Allen, T.M.; Cullis, P.R. Liposomal drug delivery systems: From concept to clinical applications. Advanced Drug Delivery Reviews. **2013**,65,36-48.

50. Dunne, M.; Zheng, J.; Rosenblat, J.; Jaffray, D.A.; Allen, C. APN/CD13-targeting as a strategy to alter the tumor accumulation of liposomes, Journal of Controlled Release. **2011**,142,298-305.

51. Torchilin, V.P. Recent advances with liposomes as pharmaceutical carriers. Drug Discovery. **2005**, 4, 145-160.

52. Pisano, C.; Cecere, S.C.; Napoli, M.D.; Cavaliere, C.; Tambaro, R.; Facchini, G.; Scaffa, C.; Losito, S.; Pizzolorusso, A.; Pignata, S. Clinical trials with peglated liposomal doxorubicin in the treatment of ovarian cancer. Journal of Drug Delivery. **2013**, 2013, 1-12.

53. Scott, R.; Crabbe, D.; Krynska, B.; Ansari, R.; Kiani, Mohammad. Aiming for the heart: targeted delivery of drugs to diseased cardiac tissue. Expert Opinion on Drug Delivery. **2008**, 5, 459-470.
54. O'Shaughnessy, J.A. Pegylated liposomal doxorubicin in the treatment of breast cancer. Clinical Breast Cancer. **2003,** 4, 318-328.
55. Fuertges, F.; Abuchowski, A. The clinical efficacy of poly(ethylene glycol) modified proteins. Journal of Controlled Release. **1990**, 11, 139-148.
56. Davis, M.E.; Chen, Z.; Shin, D.M. Nanoparticle therapeutics: an emerging treatment modality for cancer. Drug Discovery. **2008**, 7, 771-782.
57. Zebel, H.F.; Stephen, A.M. Starch: structure, analysis and application; Marcel Dekker: New York, 1996.
58. Tester, R.F.; Karkalas, J. Polysaccharides from eukaryotes; Wiley: Weinheim, 2002.
59. Tester, R.F.; Karkalas, J.; Qi, X. Starch – composition, fine structure and architecture. Journal of Cereal Science. **2004**, 39, 151-165.
60. Gallant, D.J.; Bouchet, B.; Baldwin, P.M. Microscopy of starch: evidence of a new level of granule organization. Carbohydrate Polymers. **1997**, 32, 177-191.
61. Le Corre, D.; Bras, J.; Dufresne, Alain. Starch Nanoparticles: A Review. Biomacromolecules. **2010**, 11, 1139-1153.
62. Yamamoto, M.; Takahashi, Y.; Tabata, Y. Controlled release by biodegradable hydrogels enhances the ectopic bone formation of bone morphogenetic protein. Biomaterials. **2003**,24,4375-4383.

63. Bhattarai, N.; Ramay, H.R.; Chou, S.H.; Zhang, M. Chitosan and lactic acid-grafted chitosan nanoparticles as carriers for prolonged drug delivery. Journal of International Journal of Nanomedicine. **2006**, 2, 181-187.
64. Naahidi, S.; Jafari, M.; Edalat, M.; Raymond, L.; Khademhosseini, A.; Chen, P. Biocompatibility of engineered nanoparticles for drug delivery. Journal of Controlled Release. **2013**, 166, 182-194.
65. Liu, Z.; Jiao, Y.; Wang, Y.; Zhou, C.; Zhang, Z. Polysaccharides-based nanoparticles as drug delivery systems. Advance Drug Delivery Reviews. **2008**, 60, 1650-1662.
66. Chen, S.; Liu, M.; Jin, S.; Wang, B. Preparation of ionic-crosslinked chitosan-based gel beads and effect of reaction condition on drug release behaviors. International Journal of Pharmaceutics. **2008**, 349, 180-187.
67. Tang, Y.; Xiao, S.; Zhang, J.; Guo, D.; Kong, F.; Zhang, N. Extraction of cellulose nano-crystals from old corrugated container fiber using phosphoric acid and enzymatic hydrolysis followed by sonication. Carbohydrate Polymers. **2015**, 125, 360-366.
68. Ahmad, Z.; Khuller, G.K. Alginate-based sustained release drug delivery systems for tuberculosis. Expert Opinion Drug Delivery. **2008**, 5, 1323-1334.
69. Kim, K.; Kwon, S.; Park, J.H.; Chung, H.; Jeong, S.Y.; Kwon, I.C.; Kim, I.S. Physiochemical characterization of self-assembled nanoparticles of glycol chitosan-deoxycholic acid conjugates. Biomacromolecules. **2005**, 6, 1154-1158.
70. Santander-Ortega, M.J.; Stauner, T.; Loretz, B.; Ortega-Vinuesa, J.L.; Bastos-Gonzalez, D.; Wenz, G.; Schaefer, U.F.; Lehr, C.M. Nanoparticles made from novel starch derivatives for transdermal drug delivery. Journal of Controlled Release. **2010**, 141, 85-92.

71. Tuovinen, L.; Ruhanen, E.; Kinnarinen, T.; Ronkko, S.; Pelkonen, J.; Urtii, A.; Peltonen, S.; Jarvinen, K. Starch acetate microparticles for drug delivery into retinal pigment epithelium – in vitro study. Journal of Controlled Release. **2004**, 98, 407-413.
72. Tuovinen, L.; Peltonen, S.; Jarvinen, K. Drug release from starch-acetate films. Journal of Controlled Release. **2003**, 91, 345-354.
73. Wang, S.; Copeland, L. Effect of acid hydrolysis on starch structure and functionality: A review. Food Science and Nutrition. **2015**, 55, 1079-1095.
74. Kim, J.Y.; Park, D.J.; Lim, S.T. Fragmentation of waxy rice starch granules by enzymatic hydrolysis. Cereal Chemistry. **2008**, 85, 182-187.
75. Liu, D.; Wu, Q.; Chen, H.; Chang, P.R. Transitional properties of starch colloid with particle size reduction from micro to nanometer. Journal of Colloid and Interface Science. **2009**, 339, 117-124.
76. Kim, H.Y.; Park, S.S.; Lm, S.T. Preparation, characterization and utilization of starch nanoparticles. Colloids and Surfaces B: Biointerfaces. **2015**, 126, 607-620.
77. Bloembergen, S.; McLennan, I.; Lee, D.I.; van Leeuwen, J. A starch-based biolatex can replace petroleum-based latex binders in papermaking. The Technological Association of the Pulp and Paper Industry Journal. **2008**, 46-48.
78. Klass, C. New nanoparticle laytex offers natural advantage. Paper 360°. **2007**, 30-31.
79. Lai, L.S.; Kokini, J.L. The effect of extrusion operating conditions on the on-line apparent viscosity of 98% amylopectin (Amioca) and 70% amylose (Hylon 7) corn starches during extrusion. Journal of Rheology. **1990**, 34, 1245-1266.
80. Li, D.M.H Characterization, quantification and modification of starch nanoparticles. University of Waterloo, 2014.

81. Agnihotri, S.A.; Mallikarjuna, N.N.; Aminabhavi, T.M. Recent advances on chitosan-based micro- and nanoparticles in drug delivery. Journal of Controlled Release. **2004**,100,5-28.
82. Jones, N.; Wagner, R.; Shermon, A.; Ip, A.; El-Hamed, F.; McLennan, I.; Bloembergen, S.; Liu, J. Targeted drug delivery using aptamer functionalized crosslinked starch nanoparticles.
83. Kato, Y.; Matsuo, R.; Isogai, A. Oxidation process of water-soluble starch in TEMPO-mediated system. Carbohydrate Polymers. **2003**,51,69-75.
84. Isogai, A.; Saito, T.; Fukuzumi, H. TEMPO-oxidized cellulose nanofibers. Nanoscale. **2011**, 3, 71-85.
85. Chang, P.S.; Rpbyt, J.F. Oxidation of primary alcohol groups of naturally occurring polysaccharides with 2,2,6,6,-tetramethyl-1-piperidine oxoammonium ion. Journal of Carbohydrate Chemistry. **1996**,15,819-830.
86. Hirota, M.; Tamura, N.; Saito, T.; Iogai, A. Oxidation of regenerated cellulose with $NaClO_2$ catalyzed by TEMPO and NaClO under acid-neutral conditions. Carbohydrate Polymers. **2009**, 78, 330-335.
87. Jones, N.; Wagner, R.; Shermon, A.; Ip, A.C.F.; El-Hamed, F.; McLennan, I.J.; Bloembergen, S.; Liu, J.; Targeted delivery using aptamer functionalized crosslinked starch nanoparticles.
88. Yaghoubi, H.; Khajeh, K.; Hosseinkhani, S.; Ranjbar, B.; Naderi-Manesh, H. Application of zero-length cross-linking to form lysozyme, horseradish peroxidae andlysozyme-peroxidase dimers: activity and stability. International Journal of Biological Macromolecules. **2007**, 41, 624-630.

89. Gilles M.A.; Hudson, A.Q.; Borders, C.L. Stability of water-soluble carbodiimides in aqueous solution. Analytical Biochemistry. **1990**,184,244-248.

90. Hermanson, G.T. *Bioconjugate Techniques 2nd Edition*; Elsevier: USA, 2008; p215-223.

91. Butler, J.S.; Lee, J.H.; Skalnik, D.G. PAGE separation of hemi-methylated or unmethylated oligonucleotide substrates to distinguish between maintenance and de novo DNA methyltransferase activity. Journal of Biochemical and Biophysical Methods. **2006**, 68, 195-199.

92. Mangalam, A.P; Simonsen, J.; Benight, A.S. Cellulose/DNA Hydrid Nanomaterials. Biomacromolecules. **2009**,10,497-504.

93. Ip, A.C.F.; Tsai, T.H.; Khimji, I.; Huang, P.J.J.; Liu, J. Degradable starch nanoparticle assisted ethanol precipitation of DNA. Carbohydrate polymers. **2014**, 110, 354-359.

94. Gaillard, C.; Strauss, F. Ethanol precipitation of DNA with linear polyacrylamide as carrier. Nucleic Acids Research. **1990**, 18, 378.

95. Ni, X.H.; Castanares, M.; Mukherjee, A.; Lupold, S.E. Nucleic acid aptamers: clinical applications and promising new horizons. Current Medicinal Chemistry. **2011**, 18, 4206-4214.

96. Soundararajan, S.; Chen, W.; Spicer, E.K.; Courtenay –Luck, N.; Gernandes, D.J.; The nucleolin targeting aptamer AS1411 destabilized Bcl-2 messenger RNA in human breast cancer cells. Cancer Research. **2008**, 68, 2358-2365.

97. Hwang do, W.; Ko, H.Y.; Lee, J.H.; Kang, H.; Ryu, S.H.; Song, I.C.; Lee, D.S.; Kim, S. A nucleolin-targeted multimodal nanoparticle imaging proge for tracking caner cells using an aptamer. Journal of Nuclear Medicine. **2010**, 51, 98-105.

98. Ireson, C.R.; Kelland, L.R. Discovery and development of anticancer aptamers. Molecular Cancer Therapeutics. **2006**, 5, 2957-2962.

99. Hovanessian, A.G.; Puvion-Dutilleul, F.; Nisole, S.; Svab, J.; Perret, E.; Deng, J.S.; Krust, B. The cell-surface-expressed nucleolin is associated with actin cytoskeleton. Experimental Cell Research. **2000**, 261, 312-328.

100. Shangguan, D.H.; Li, Y.; Tang, Z.; Cao, Z.C.; Chen, H.W.; Mallikaratchy, P.; Sefah, K.; Ynag, C.J.; Tan, W. Aptamers evolved from live cells as effective molecular probes for cancer study. Proceedings of the National Academy Sciences. **2006**, 103, 11838-11843.

101. Xiao, Z.Y.; Shangguan D.H.; Cao, Z.H.; Fang, X.H.; Tan, W.H. Cell specific internalization study of an aptamer from whole cell selection. Chemistry-A European Journal. **2008**, 14, 1769-1775.